

See discussions, stats, and author profiles for this publication at: <https://www.researchgate.net/publication/366498200>

Antioxidant, Antibacterial, and BSA Binding Properties of Curcumin Caffeate Capped Silver Nanoparticles Prepared by Greener Method

Article in *ChemistrySelect* · December 2022

DOI: 10.1002/slct.202203989

CITATIONS

0

READS

124

4 authors, including:



Nishi Gandha Gogoi

MDKG College

6 PUBLICATIONS 8 CITATIONS

[SEE PROFILE](#)



Pankaj Dutta

Dibrugarh University

32 PUBLICATIONS 221 CITATIONS

[SEE PROFILE](#)

Antioxidant, Antibacterial, and BSA Binding Properties of Curcumin Caffeate Capped Silver Nanoparticles Prepared by Greener Method

Nishi Gandha Gogoi,^[a] Pankaj Dutta,^[b] Jiban Saikia,^{*[a]} and Jyotirekha G. Handique^{*[a]}

A green method of silver nanoparticle (AgNP) preparation using curcumin caffeate (CCaf) as stabilizing/capping and reducing group is reported here. CCaf is prepared through esterification of curcumin and caffeic acid in presence of *p*-toluene sulphonic acid as catalyst. CCaf facilitates production of AgNPs in aqueous medium and room temperature without any external reducing agents. The antioxidant, antibacterial and BSA binding interactions of these CCafAgNPs are evaluated. The antioxidant activity and the corresponding IC₅₀ value for the CCafAgNPs is found to be comparable with ascorbic acid

taken as standard antioxidant for the study. The results of bactericidal screening of CCafAgNPs are better compared to CCaf capping group and found to exhibit broad spectrum antibacterial property against Gram-positive and Gram-negative bacterial pathogens. In presence of CCafAgNPs the absorption spectra of BSA showed changes with increase in intensity around 280 nm of native BSA peak and appearance of a new band around 320 nm, indicating the possible binding interactions between BSA and CCafAgNPs.

Introduction

Nanoparticles are gaining utmost attention in the 21st century for their diverse applications in catalytic, optoelectronics, electrical, biomedicine and pharmaceutical fields.^[1–4] Silver nanoparticles (AgNPs) have beneficial properties and applications in biotechnology and medicinal ground as antioxidants, anti-inflammatory drugs, antibiotics, and biosensors, and hence are most intensively studied in the recent decades.^[5–8] The antibacterial and anti-inflammatory properties of AgNPs finds use in medicine to reduce or inhibit bacterial growth on human skin and medical equipment, burns and wounds, water treatment and textiles.^[9,10] Often, AgNPs have the tendency to agglomerate, resulting in increase in particle size and decrease in their surface energy and beneficial usability.^[11] AgNPs without a support/capping group is hard to recover and reuse. The morphology of the AgNPs including their shape and size and type of capping material used, is important in tuning the properties of AgNPs.^[12] Therefore, researchers are involved in extensive studies for developing new and improved synthesis methods for regulating the morphology of AgNPs.

Considering the environmental disadvantages of the conventional chemical and physical methods green methodologies

are developed in preparing AgNPs in recent times. Chemical reduction, laser synthesis, photo reduction, etc. are energy and time consuming and require strict preparation conditions.^[13–15] At the same time, some of these methods incorporate use of hazardous chemicals as hydrazines or borohydrides as reducing agents, and release environmentally contaminated byproducts.^[16,17] The production of AgNPs by toxic conditions is a critical concern and threat to the environment and so, replacement by safe and sustainable alternatives are gaining importance. Utilization of plant extracts and their components are gathering interests of the scientists as an easy, fast, economic, and environment sustainable technique for production of AgNPs.^[18–20]

Plant based components such as polyphenols, polymers and hydrogels are non-toxic and biodegradable and therefore, are explored and preferred as capping and reducing agents in preparation of metallic nanomaterials,^[21,22] over the synthetic polymers such as polyvinylchloride (PVC), polyacrylamides, polyurethanes (PU), and polyethylene glycols (PEGs), ionic surfactants such as sodium dodecyl sulphate (SDS) and non-ionic surfactants such as Brij, Tween, etc.^[23–26] Polyphenols such as curcumin and hydroxycinnamic acids possess no toxicity issues to human health and so their antioxidant, anti-bacterial, anti-cancer, anti-inflammatory, and anti-alzheimer activities are explored over many years.^[27–29] Curcumin, a natural yellow-orange compound, extracted from the roots of *Curcuma longa* rhizome and is used in medicinal applications by oriental cultures.^[28] Hydroxycinnamic acids includes caffeic, coumaric, ferulic, and sinapic acids which are mostly found in plants and plant products such as cereals, legumes, fruits, vegetables, and oilseeds. Caffeic acid is mainly found in plants and their products such as coffee, tea, wine, etc.^[30] In addition to the proven medicinal properties, curcumin and its derivatives have been used as reducing and capping agent in AgNP production.^[31–34] These curcumin capped AgNPs are reported to

[a] N. Gandha Gogoi, Dr. J. Saikia, Prof. Dr. J. G. Handique
Department of Chemistry
Dibrugarh University
786004 Dibrugarh, Assam, India
E-mail: jghandique@dibru.ac.in
ngogoi28@gmail.com

[b] Prof. Dr. P. Dutta
Department of Physics
Dibrugarh University
786004 Dibrugarh, Assam, India


 Supporting information for this article is available on the WWW under <https://doi.org/10.1002/slct.202203989>

exhibit antimicrobial and antioxidant properties that can be exploited in designing food packaging and wound healing material.^[35,36]

In the course of using nanoparticles for medical purposes, the nanoparticles are applied/released to the protein surfaces for binding and delivering at the target site.^[37] Many forces such as vander Waals forces, hydrogen bonding, and hydrophobic interactions are involved in the process of adsorption of NPs on the surface of protein and forming a layer.^[38] It is important to understand the nature of interactions that develops between the protein and NPs for exploring the effects of binding of NPs on structure and stability of protein and safe drug delivery at the expected target site.^[39] For this purpose, bovine serum albumin (BSA) is mostly employed. Serum albumins are abundantly available in blood plasma and are involved in transport of various exogenous and endogenous compounds.^[40] BSA has 583 amino acid residues and the secondary structure consists of mainly α helices and the remaining are β sheets, twists and coils. It has three domains I, II and III with two subdomains A and B each. There are two tryptophan (Trp124 and Trp 213) and phenylalanine (Phe) residues at the binding site.^[41]

To the best of our knowledge, curcumin caffeate capped AgNPs and the evaluation of their biomedical properties are not reported earlier. In this work, we synthesized curcumin caffeate derivative of curcumin and used it as reducing and capping agent in AgNPs production in aqueous medium and room conditions without use of any external mechanical applications. The antioxidant behaviour of AgNPs is measured by DPPH assay. Bactericidal property is screened for Gram-positive bacteria -Staphylococcus aureus, and Gram-negative bacteria – Escherichia coli, Klebsiella pneumoniae, Acinetobacter baumannii, and Pseudomonas aeruginosa. The drug-protein binding interaction between BSA and AgNPs is studied by UV-visible and fluorescence spectrophotometer.

Results and Discussion

Curcumin caffeate (CCaf) was prepared by Knoevenagel condensation between curcumin and caffeic acid. Briefly, curcumin (1 mM) and caffeic acid (2 mM) is dissolved in ethanol and refluxed for 6 hours in presence of para-toluene sulphonic acid (p-TSA) as catalyst. The reaction was monitored by recording thin layer chromatography (TLC) plates at different time intervals. The extra solvent was removed and the product was extracted, washed with aqueous base and acid solutions, filtered, dried in sodium sulphate and purified by column chromatography. The characterization of CCaf was done by using FT-IR, ^1H and ^{13}C NMR and LCMS spectrometric techniques. Furthermore, CCaf was used in easy and green preparation of AgNPs from AgNO_3 in aqueous medium and at room temperature (27°C). Most of the methods reported in literature often require high preparation temperature, long reaction time, external equipment or toxic reducing agents.^[42] In the present silver nanoformulation procedure, CCaf as capping and reducing complex completes the AgNPs production in safe and

simple operating eco-friendly conditions, consuming less (or no) energy and solvent and without producing waste.

The surface plasmon resonance (SPR) phenomenon of the synthesized AgNPs on CCaf as stabilizer was characterized by monitoring the absorbance spectrum at different time intervals in UV-visible spectral region. AgNPs are reported to yield a SPR absorption band in the visible region around 400 nm due to the resonance of their free electrons with the photons in that spectral region. Figure 1 depicts the absorption spectrum of CCafAgNPs recorded at different time intervals during the synthesis procedure. In the initial stages of synthesis, AgNO_3 dissociates releasing Ag^+ and NO_3^- ions in aqueous medium. The hydroxyl groups on CCaf encapsulate the silver ions when it was added to the reaction medium followed by reduction of Ag ions to give the CCafAgNPs. Physical changes observed in the colour from yellow to dark green indicate the formation of AgNPs, confirmed by a SPR band at 424 nm, reduced and stabilized by CCaf complex.

The sharp and intense distinct peaks XRD pattern shows the crystallinity of the AgNPs (Figure 2). The peaks at 38:18, 44:29, 64:43, and 77:48 are well indexed to the 111, 200, 220 and 311 planes of silver, respectively and are in good agreement with the face centered cubic (FCC) lattice structure Ag

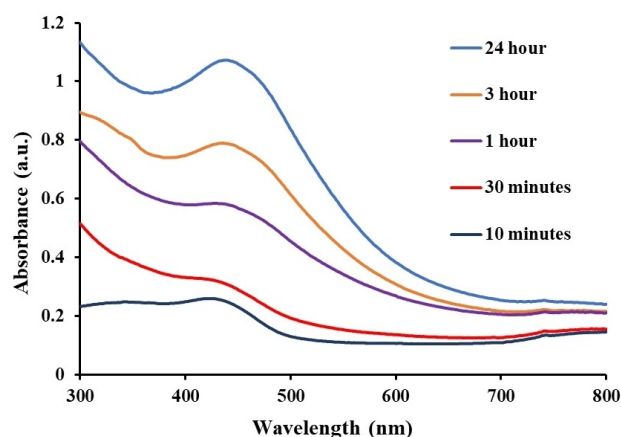


Figure 1. Absorption spectrum of CCaf-AgNPs at different time intervals.

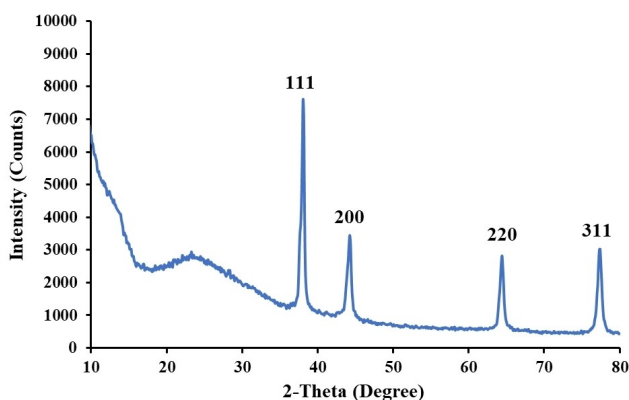


Figure 2. XRD pattern of CCafAgNPs.

(JCPDS silver file No. 04-0783).^[43] The relatively high intense signal is that of 111 Bragg's reflection and reveals its exposure in the structure. Presence of no other signals indicates the purity of sample. The elemental EDX profile shown in Figure 3, demonstrates a sharp signal of silver at 3 keV, confirming the major element in the NPs as silver. Along with silver, prominently distinguishable peaks of oxygen, carbon and chlorine are observed in the EDX pattern in the signal range of 0–0.5 keV. This confirms the presence of CCaf as capping agent on the surface of AgNPs that tends to prevent aggregation of AgNPs.

The morphology of the surface of AgNPs and their particle shape and size distribution are demonstrated by the SEM (Figure 3) and TEM results. High resolution TEM images showed that the AgNPs formed by CCaf are relatively spherical in shape. The crystallite size of CCafAgNPs estimated from Debye Scherrer's formula is 30 nm with interplanar spacing of 0.235 nm corresponding to the 111 plane (Figure 4a). The highly-dense AgNPs are homogeneously distributed. The selected area electron diffraction (SAED) pattern (Figure 4b) shows crystalline nature of AgNPs and spotty rings corresponds to the 111, 200, 220 and 311 planes, as observed in XRD profile.

Antioxidant activity

The free radicals and reactive oxygen species, generated from cellular oxidation are responsible for adverse cellular damage and chronic diseases. The reactive radical species as H_2O_2 , $\bullet\text{O}_2^-$ (superoxide anion), OH (hydroxyl radical), NO and $^1\text{O}_2$ (singlet oxygen) are responsible for causing damage at the cellular and tissue sites by injuring the peptides, nucleic acids, and lipids in inflammatory cells leading to chronic health conditions. Antioxidants are known to decelerate these devastating effects by neutralizing these free radicals and species.^[44] The antioxidant activity of CCafAgNPs is evaluated through DPPH assay shown in Figure 5. Ascorbic acid is used as a standard antioxidant. The antioxidant capacity of the CCafAgNPs is found to increase with its increasing concentration resulting in enhanced ability to scavenge DPPH radical. The IC_{50} values are calculated from the plot of % inhibition versus concentration

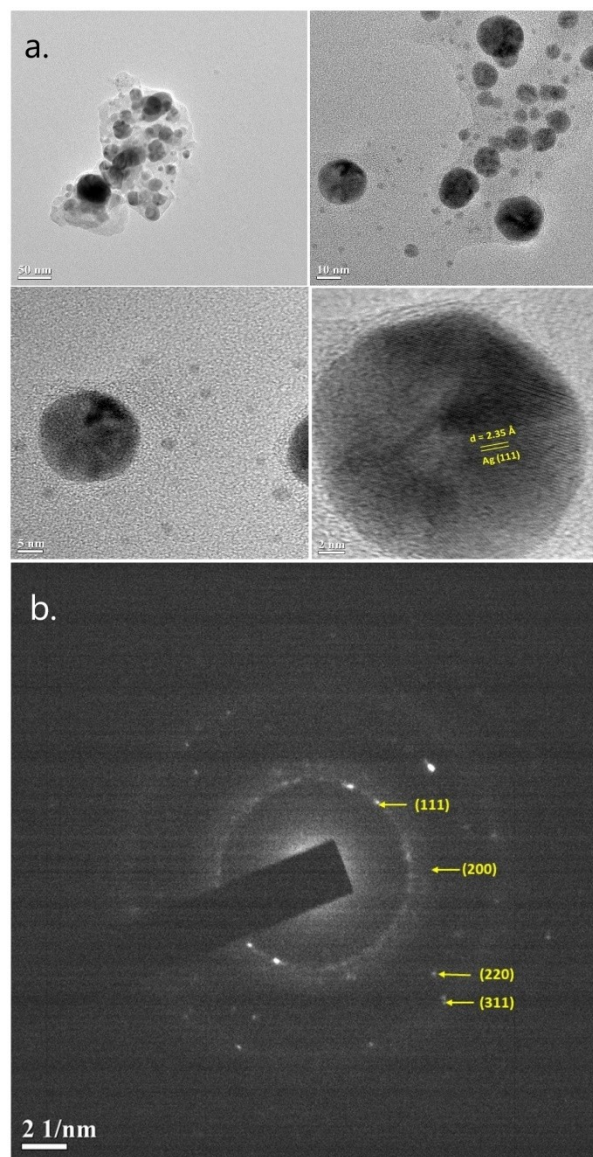


Figure 4. a. TEM images, and b. SAED pattern of CCafAgNPs.

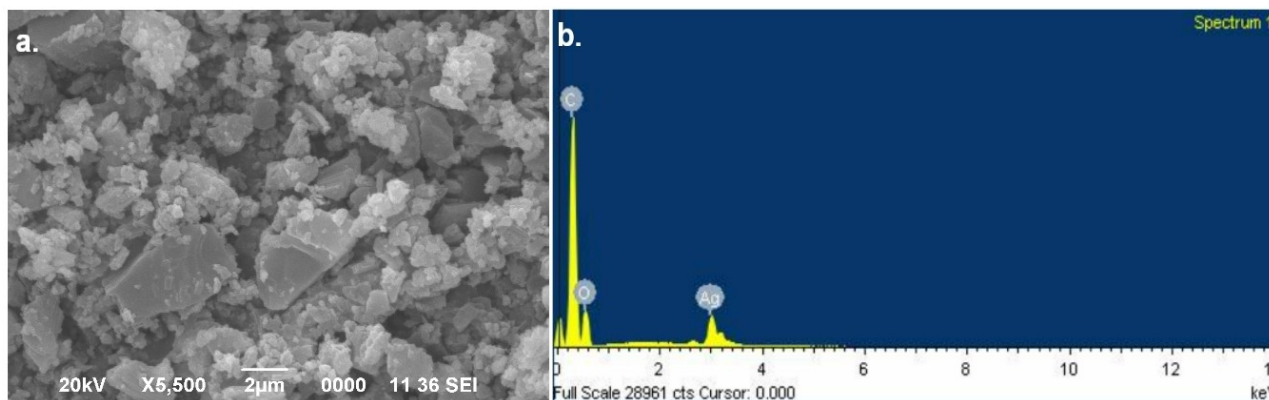


Figure 3. Scanning electron microscopy (SEM), and energy dispersive X-ray (EDX) analysis of CCafAgNPs.

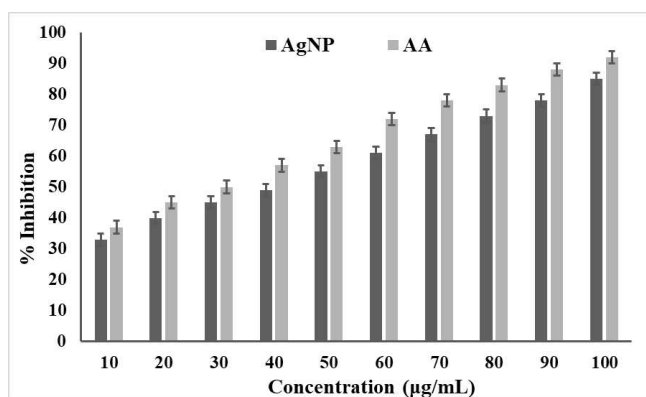


Figure 5. DPPH radical scavenging activity of CCafAgNPs (AgNP) and ascorbic acid (AA) as standard antioxidant.

graph. Although antioxidant capacity of AgNPs is lower than ascorbic acid, but their IC_{50} values are quite comparable i.e., 57.13 $\mu\text{g/mL}$ for AgNPs, and 45.40 $\mu\text{g/mL}$ for ascorbic acid. The observed antioxidant behaviour of AgNPs is accounted for the presence of hydroxyl groups present on the capping group.

BSA binding study

UV-visible absorbance

The interaction of BSA and CCafAgNPs is observed from the UV-visible absorption and steady state fluorescence spectra measurements. In absence of CCafAgNPs, BSA shows two absorption peaks at 200–230 nm (corresponding to $\pi \rightarrow \pi^*$ transition of polypeptide chain) and 260–290 nm due to $n \rightarrow \pi^*$ transition of the Tyr/Trp chromophores.^[45] The intensity of the absorption peak of BSA around 280 nm is found to change in presence of CCafAgNPs with the appearance of a new band around 320 nm, shown in figure 6. The intensity of the peak increases with increase in the concentration from 10–100 $\mu\text{g/mL}$ of AgNPs. The hypsochromic shift is due to formation of a ground state complex between BSA and CCafAgNPs.^[46] Similar results of BSA and nanoparticles are reported in literature.^[47] These changes clearly indicate the interaction of BSA and CCafAgNPs and change in the microenvironment near Trp, Tyr and Phe residues located in the binding cavity of BSA. The

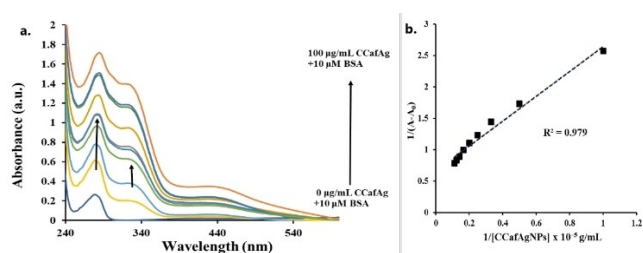


Figure 6. a. Absorption spectrum of BSA-CCafAgNPs binding interactions; b. Benesi-Hildebrand plot of $1/(A-A_0)$ versus $1/[\text{CCafAgNPs}]$.

nature of quenching of BSA in presence of AgNPs is static in this case,^[47] as indicated by the change of absorption spectra of BSA. The polar and hydrophobic interactions between the hydroxy groups and aromatic moieties of CCaf and polar and hydrophobic amino acid residues on BSA respectively, are responsible for the observed binding interactions. The binding constant, K_{app} of CCafAgNPs-BSA protein from absorbance spectrum is calculated from the Benesi-Hildebrand plot (equation 1) of $1/(A-A_0)$ versus $1/[\text{CCafAgNPs}]$ and found to be $3.52 \times 10^4 \text{ M}^{-1}$.

$$\frac{1}{(A-A_0)} = \frac{1}{(A_C-A_0)} + \frac{1}{K_{\text{app}}(A_C-A_0)} \times [\text{CCafAgNPs}] \quad (1)$$

where, A is the absorbance observed for BSA with different concentrations of ligand; A_0 is the blank absorbance of BSA; A_C is the maximum absorbance of BSA with ligand; K_{app} is the apparent binding constant. A graph of $1/(A_{\text{obs}}-A_0)$ versus $1/[\text{CCafAgNPs}]$ the ratio of intercept to slope of the linear fit plot gave the K_{app} of BSA and ligand.

Steady state fluorescence emission

The quenching of emission intensity of a fluorophore in presence of a complex occurs due to various molecular interactions such as molecular rearrangements, energy transfer, excited state reactions, collisions among molecules (dynamic quenching) or formation of ground state complex (static quenching).^[48] BSA shows fluorescence for the presence of three intrinsic fluorophores in their structure- Phe, Tyr and Trp. Trp is considered as the main contributor of showing fluorescence in BSA as Phe and Tyr are opted out for low fluorescence quantum yield and high fluorescence quenching in presence of amino/carboxyl group, respectively.^[49] The fluorescence quenching is important in establishing the binding interaction of BSA in presence of ligands as Trp residue is highly responsive to the minor change in hydrophobicity or polarity in its surrounding.^[50] It is observed that the fluorescence intensity of BSA diminishes with increase in concentration of ligands. Figure 7 shows the fluorescence emission spectra of CCafAgNPs and BSA and the corresponding Benesi-Hildebrand plot of $1/(F_0-F)$ versus $1/[\text{CCafAgNPs}]$ for BSA where F_0 is the fluorescence intensity of BSA in absence of ligand and F is the fluorescence intensity in presence of ligand. The K_{app} value of BSA-CCafAgNPs binding from fluorescence spectra is found to be $9.02 \times 10^4 \text{ M}^{-1}$.

Stern-Volmer equation (equation 2) explains the nature of mechanism of protein-ligand quenching i.e., whether it is static quenching or dynamic quenching.

$$F_0/F < C \Rightarrow K_{\text{sv}} [\text{CCafAgNPs}] + 1 \quad (2)$$

$$K_{\text{sv}} = K_q \tau_0 \quad (3)$$

where, F and F_0 are the fluorescence intensity of serum albumins in the presence and absence of CCafAgNPs as

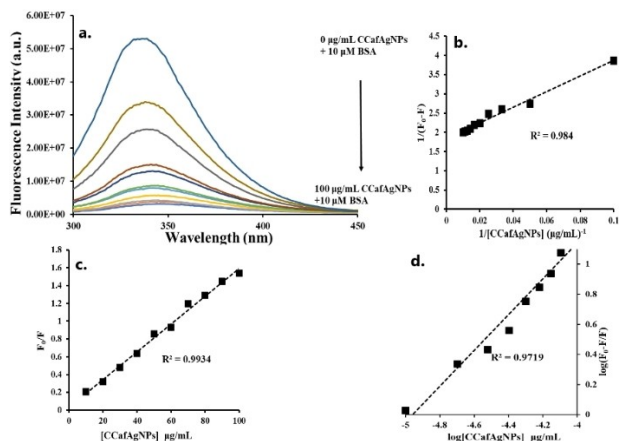


Figure 7. a. Fluorescence emission spectrum of BSA-CCafAgNPs with increasing concentration of CCafAgNPs (0–100 µg/mL); b. Benesi-Hildebrand plot of $1/(F_0 - F)$ versus $1/[CCafAgNPs]$; c. Stern-Volmer plot of F_0/F versus $[CCafAgNPs]$; d. double logarithmic modified Stern-Volmer plot.

quencher and K_{SV} is Stern-Volmer constant. The quenching constant, K_q is the ratio of K_{SV} and τ_0 (average lifetime of BSA; 10^{-8} s for BSA).^[51] The slope of the linear Stern-Volmer plot of F_0/F vs. $[CCafAgNPs]$ of BSA is equal to the value of K_{SV} ($0.156 \times 10^5 M^{-1}$). The calculated K_q value is $1.56 \times 10^{12} M^{-1}s^{-1}$ and is greater than collision quenching constant $2.0 \times 10^{10} M^{-1}s^{-1}$.^[52] This confirms quenching mechanism to be static quenching for formation of ground state complex between BSA and CCafAgNPs. The ground state complex formed is stabilised by non-covalent interactions as electrostatic, van der Waals or hydrophobic forces and formation of hydrogen bonds.^[53]

The number of binding sites between BSA and CCafAgNPs is given by modified Stern-Volmer electrostatic equation (equation 3)

$$\log\left(F_0 - \frac{F}{F}\right) = n \log[CCafAgNPs] + \log K_{app} \quad (4)$$

n is the number of binding sites between CCafAgNPs and BSA calculated from the linear plot of $\log(F_0 - F/F)$ versus $\log[CCafAgNPs]$. CCafAgNPs are found to uniquely bind to BSA ($n = 1.191$). The spectroscopic results from fluorescence and UV-visible is found to be in good agreement with formation of

ground state complex and can be concluded from the observed changes of both the spectroscopic analysis.

Antibacterial activity

The bactericidal property of CCafAgNPs, CCaf and curcumin is screened against both Gram positive bacteria – *S. aureus* ATCC 29213, and Gram-negative bacteria – *E. coli* ATCC 25922, *K. pneumoniae* BAA 1705, *A. baumannii* BAA 1605, and *P. aeruginosa* ATCC 27853 by evaluating the minimum inhibitory concentration (MIC) values of AgNPs by microbroth dilution assay. Levofloxacin is used as a standard antibiotic. CCafAgNPs are found to exhibit broad-spectrum antibacterial activity against these bacterial pathogens and are more effective than curcumin and CCaf (capping agent), as shown in Table 1, due to the presence of Ag metal. The positive charge on CCafAgNPs is attracted by the negative charge on bacterial cell wall leading to the releasing of silver ions through pore formation inside the bacterial cell membranes. Inside the membrane, the affinity of silver ions for sulphur and phosphorus containing macromolecules results in disruption of ATP production and DNA replication. AgNPs also causes oxidative stress inside bacterial cell membrane by triggering the generation of free radicals ultimately leading to cell death.^[54–57] The combinatorial action of the AgNPs on bacterial cell accounts for their inhibitory effect as antibacterial compounds.

Conclusion

In this work, AgNPs capped and reduced by curcumin caffeate (CCaf) polyphenol is prepared for the first time by cost-effective and greener method. The stabilized AgNPs are characterized by XRD, SEM-EDX and TEM analytical techniques. The fabricated nanomaterial is found to have a face centred cubic lattice and average size of each particle is found to be 30 nm. The biological properties of CCafAgNPs are evaluated and found to have effective antioxidant, and antibacterial properties which may be used further in pharmaceutical fields, or in sterilization procedures. CCafAgNPs are found to be effective against both gram-positive and gram-negative bacterial pathogens (compared to curcumin and CCaf) which makes CCafAgNPs eligible to be used in food packaging materials as sensors for microbial contamination. The BSA-nanoparticle interactions have also been studied by UV-visible and fluorescence emission spectroscopic methods. The BSA-CCafAgNPs binding interaction study may provide initial insight in nanobiotechnology and designing

Table 1. Minimum Inhibitory Concentration (MIC in µg/ml) of CCafAgNPs, CCaf and curcumin on tested bacterial pathogens (triplicate studies). DMSO is used as the negative control and Levofloxacin as the positive control. ‘-’ indicate no activity.

Drug	Minimum inhibitory concentration (MIC in µg/ml)				
	<i>E. coli</i> ATCC 25922	<i>S. aureus</i> ATCC 29213	<i>K. pneumoniae</i> BAA 1705	<i>A. baumannii</i> BAA 1605	<i>P. aeruginosa</i> ATCC 27853
CCafAgNPs	64	64	> 64	64	64
CCaf	> 64	64	> 64	> 64	> 64
Curcumin	> 64	> 64	> 64	> 64	> 64
Levofloxacin (Std)	0.0156	0.25	64	8	1
DMSO	-	-	-	-	-

new drugs and further detailed study in this domain are needed.

Experimental Section

Methods

UV-visible absorption and Fluorescence spectrophotometry

The SPR phenomenon of AgNPs resulting from reduction of Ag^+ ions by CCaf are monitored by Hitachi U-3900H UV-visible spectrophotometer and HORIBA Fluoromax-4 fluorescence spectrophotometer. The analysis is performed using distilled water as reference in quartz cuvettes and diluting 1 mL of AgNPs suspension 4 mL of distilled water.

Fourier transform infrared spectra (FTIR)

FTIR spectra is recorded in the range of 400–4000 nm with a Shimadzu IRPrestige-21 FTIR spectrophotometer on KBr palletes.

Nuclear magnetic resonance (NMR)

^1H and ^{13}C NMR spectra are recorded by a Bruker Advance II spectrophotometer at 400 MHz and 100 MHz, respectively in DMSO-d_6 solvent and TMS as internal standard.

Molecular mass spectra

Molecular mass of CCaf is measured by a Ultimate 3000/TSQ Endura liquid chromatograph mass spectrometer (LCMS).

Powder X-ray diffraction (XRD)

XRD pattern is recorded with a Bruker AXS D8 Focus X-ray diffractometer by irradiating monochromatic $\text{Cu-K}\alpha$ (1.541 Å radiation).

Transmission electron microscopy (TEM)

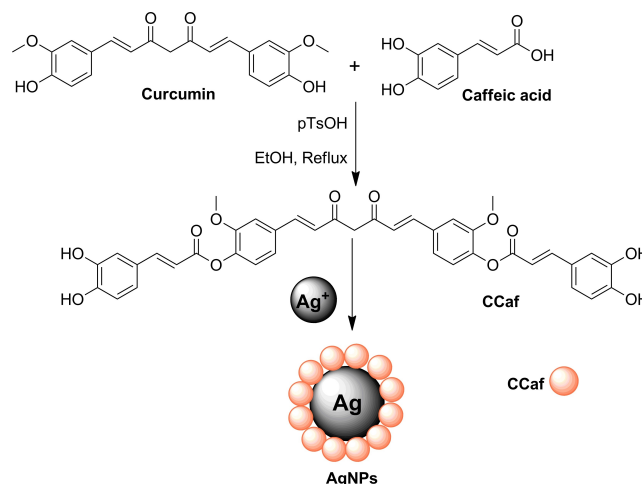
Transmission electron Microscopy (TEM) and selected area diffraction (SAED) analysis of stabilized AgNPs is performed with a JEM-100 CX II transmission electron microscope equipped operating at 20–100 KV in 20 KV steps having high resolution CCD camera from 3 Å to 1.4 Å.

Scanning electron microscopy (SEM)

Scanning electron microscopy (SEM) and energy dispersive X-ray (EDX) spectra is recorded in JEOL/JSM 6390LV scanning electron microscope.

Synthesis of curcumin caffeate (CCaf)

Curcumin caffeate is prepared by the method reported earlier. Briefly, a mixture of curcumin (1 mM) and caffeic acid (2 mM) in ethanol is refluxed for 6 h at 60 °C in presence of p-TsOH and under nitrogen atmosphere with constant stirring. The completion of the reaction is monitored by examining TLC. The solvent is removed under reduced pressure using rotatory evaporator, and the product so formed is purified by column chromatography (Scheme 1).



Scheme 1. Preparation of CCaf from curcumin and caffeic acid and AgNPs reduced/capped by CCaf.

Characterization is done by FTIR, ^1H and ^{13}C NMR and LCMS analysis.

(2E,2'E)-((1E,6E)-3,5-dioxohepta-1,6-diene-1,7-diyl)bis(2-methoxy-4,1-phenylene)bis(3-(3,4-dihydroxyphenyl)acrylate) (CCaf)

Light orange solid. Yield: 0.486 g (70.2%). ^1H NMR (400 MHz, DMSO-d_6) δ 7.50 (d, $J = 12$ Hz, =C–H), 7.26 (s, Ar–H), 7.12 (dd, $J = 4$ Hz, 4 Hz, Ar–H), 6.80 (d, $J = 12$ Hz, Ar–H), 6.71 (d, $J = 16$ Hz, =C–H), 6.63 (m, Ar–H), 6.58 (m, Ar–H), 6.40 (d, $J = 16$ Hz, =C–H), 6.05 (s, Ar–H), 5.84 (s, Ar–OH), 4.11 (s, – CH_2), 3.79 (m, – OCH_3); ^{13}C NMR (100 MHz, DMSO-d_6) δ 183.08 (–C=O), 168.56 (–O–C=O), 149.38 (–C– OCH_3), 147.52 (–C– OCH_3), 145.54 (–C–OH), 140.36 (Ar–C), 130.53 (Ar–C), 128.69 (Ar–C), 126.84 (C=), 125.35 (–C=), 123.02 (Ar–C–O–C=O), 121.16 (–C=), 116.00 (Ar–C), 111.32 (Ar–C), 108.50 (Ar–C), 102.85 (Ar–C), 101.48 (Ar–C), 55.43 (– OCH_3), 51.75 (– CH_2); LCMS (m/z): 690.44 [$\text{M}-2\text{H}$]⁺ (Calculated $\text{M}^+ = 692.19$).

Preparation of CCaf stabilized silver nanoparticles (green synthesis)

To a 1 mM aqueous silver nitrate (AgNO_3) solution (10 mL) at ambient temperature, 0.1 mM of CCaf is added. The reaction mixture turns brown colour, indicating the start of reduction process of Ag^+ ions and development of AgNPs. The progress of the process of formation of AgNPs is monitored by UV-visible spectrophotometer. The mixture is centrifuged, washed with ethanol/water and dried to obtain the stabilized AgNPs (Scheme 1). The in-vitro antioxidant and antibacterial properties, and BSA -drug binding study of these CCafAgNPs are evaluated.

Antioxidant activity

The antioxidant property of CCaf-AgNPs is measured by DPPH-radical scavenging assay following the method described by Brand-Williams et al. with some modifications.^[58] AgNPs solution of concentrations 10–100 $\mu\text{g/mL}$ in distilled water are prepared and mixed with 100 μM methanolic solution of DPPH. The reaction mixture is kept in the dark at room temperature for 30 minutes.

The absorbance of the reaction mixture is measured by UV-visible spectrophotometer at 517 nm in parallel with a reagent blank. The percent inhibitions of DPPH• by the antioxidants are measured by the bleaching of the purple colour of DPPH. The % inhibition is calculated as

$$\% \text{ DPPH} \cdot \text{inhibition} = ((A_b - A_e)/A_b) \times 100 \% \quad (5)$$

where, A_b is the absorbance of the blank reagent and A_e is the absorbance of the reaction mixture. Ascorbic acid is used as a standard. The results are shown as percentage (%) inhibition versus the concentrations CCafAgNPs.

BSA binding study

The BSA binding interactions with CCafAgNPs is studied UV-visible and fluorescence spectrophotometer by the change in absorption or emission spectra of BSA^[59] in presence of increasing concentrations of CCafAgNPs as ligand (10–100 µg/mL). The reaction mixture consists of 2 mL of BSA (10 µM) in phosphate buffer solution (PBS, pH 7.4), 0.5 mL of PBS and 0.5 mL of CCafAgNPs solution. The mixture is incubated at 37°C for 30 minutes before recording spectroscopic data. The binding constant (K_{app}) is evaluated from absorption data by Benesi-Hindelbrand equation (equation 6).

$$1/(A - A_0) = 1/(A_C - A_0) + 1/K_{app} (A_C - A_0) [\text{ligand}] \quad (6)$$

where, A is the absorbance observed for BSA with different concentrations of ligand; A_0 is the blank absorbance of BSA; A_C is the maximum absorbance of BSA with ligand; K_{app} is the apparent binding constant. A graph of $1/(A_{obs} - A_0)$ versus $1/[CCafAgNPs]$ and $1/(F_0 - F)$ versus $1/[CCafAgNPs]$ and the ratio of intercept to slope of the linear fit plot gave the K_{app} of BSA and ligand.

Antibacterial activity

The bactericidal property of CCafAgNPs is screened for ESKAPE pathogen panel- Escherichia coli ATCC 25922, Staphylococcus aureus ATCC 29213, Klebsiella pneumoniae BAA 1705, Acinetobacter baumannii BAA 1605, and Pseudomonas aeruginosa ATCC 27853 by microbroth dilution method.^[60] The results are expressed in terms of minimum inhibitory concentration (MIC) values in µg/mL. AgNPs of different concentrations (0–64 µg/mL) in DMSO is taken in different wells. Bacteria culture, grown in 5% Muller-Hinton broth for 18 h are rinsed with sterile phosphate buffer solution twice and diluted to $\sim 5 \times 10^5$ CFU/mL. Levofloxacin is used as standard antibiotic.

Supporting Information Summary

The spectroscopic data of the capping agent CCaf is included in the supplementary information.

Acknowledgements

We are grateful to the UGC, New-Delhi for Special Assistance Program (SAP-DRS) and Department of Science and Technology (DST), Govt. of India, for financial assistance under DST-FIST programme to the Department of Chemistry, Dibrugarh Univer-

sity. N. G. G. acknowledges DURF, Dibrugarh University for financial assistance. We acknowledge SAIC Tezpur University for SEM, EDX and XRD analysis, SAIF NEHU, Shillong for TEM analysis, and CDRI Lucknow for antibacterial screening tests.

Conflict of Interest

The authors declare no conflict of interest.

Data Availability Statement

The data that support the findings of this study are available from the corresponding author upon reasonable request.

Keywords: Antioxidant · Antibacterial · BSA binding · Curcumin caffeate · Silver nanoparticles

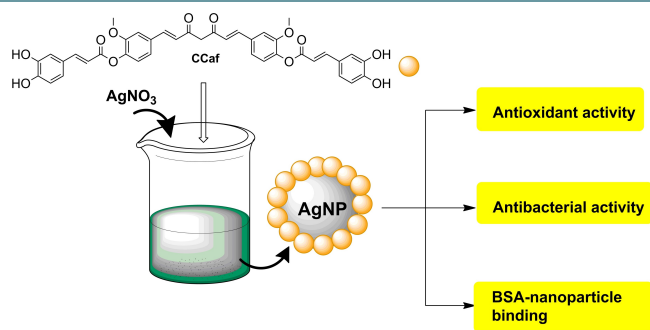
- [1] H. Barani, M. N. Boroumand, S. Rafiei, *Fibers Polym.* **2017**, *18*, 658–665.
- [2] Z. Zhang, W. Shen, J. Xue, Y. Liu, P. Yan, J. Liu, J. Tang, *Nanoscale Res. Lett.* **2018**, *13*, 54–72.
- [3] J. Zhang, S. Li, *Int. J. Environ. Anal. Chem.* **2019**, *101*, 1–23.
- [4] V. Vorobyova, G. Vasyliov, M. Skiba, *Appl. Nanosci.* **2020**, *10*, 4523–4534.
- [5] A. K. Potbhare, P. B. Chouke, A. Mondal, R. U. Thakare, S. Mondal, R. G. Chaudhary, A. R. Rai, *Mater. Today: Proc.* **2020**, *29*, 939–945.
- [6] A. K. Keshari, R. Srivastava, P. Singh, V. B. Yadav, G. Nath, *J. Ayurveda Integr. Med.* **2020**, *11*, 37–44.
- [7] M. Alavi, R. S. Varma, *Cellulose* **2021**, *28*, 8295–8311.
- [8] Z. Li, W. Ma, I. Ali, H. Zhao, D. Wang, J. Qiu, *ACS Omega* **2020**, *5*, 32632–32640.
- [9] S. Islam, B. S. Butola, A. Kumar, *Int. J. Biol. Macromol.* **2020**, *152*, 1135–1145.
- [10] K. Kalantari, E. Mostafavi, A. M. Affi, Z. Izadiyan, H. Jahangirian, R. Rafiee-Moghaddam, T. J. Webster, *Nanoscale* **2020**, *12*, 2268–2291.
- [11] X. Li, J. J. Lenhart, H. W. Walker, *Langmuir* **2012**, *28*, 1095–1104.
- [12] V. Bansal, V. Li, A. P. O'Mullane, S. K. Bhargava, *CrystEngComm* **2010**, *12*, 4280–4286.
- [13] S. Agnihotri, S. Mukherji, S. Mukherji, *RSC Adv.* **2014**, *4*, 3974–3983.
- [14] J. Kwon, J. Yeo, S. Hong, Y. D. Suh, H. Lee, J. Choi, S. S. Lee, S. H. Ko, *Energy Technol.* **2016**, *4*, 271–277.
- [15] H. Wang, X. Qiao, J. Chen, S. Ding, *Colloids Surf. A* **2005**, *256*, 111–115.
- [16] V. Gurusamy, R. Krishnamoorthy, B. Gopal, V. Veeraravagan, P. Neelamegam, *Inorg. Nano-Met. Chem.* **2017**, *47*, 761–767.
- [17] K. Mavani, M. Shah, *Int. J. Eng. Res. Technol.* **2013**, *2*, 1–5.
- [18] S. Ansar, H. Tabassum, N. S. M. Aladwan, M. N. Ali, B. Almaarik, S. AlMahrouqi, M. Abudawood, N. Banu, R. Alsubki, *Sci. Rep.* **2020**, *10*, 18564.
- [19] S. Jadoun, R. Arif, N. K. Jangid, R. K. Mehta, *Environ. Chem. Lett.* **2021**, *19*, 355–374.
- [20] C. Vanlalveni, S. Lallianrawna, A. Biswas, M. Selvaraj, B. Changmai, S. L. Rokhum, *RSC Adv.* **2021**, *11*, 2804–2837.
- [21] P. B. Chouke, A. K. Potbhare, K. M. Dadure, A. J. Mungole, N. P. Meshram, R. R. Chaudhary, A. R. Rai, R. G. Chaudhary, *Mater. Today: Proc.* **2020**, *29*, 720–725.
- [22] A. K. Potbhare, R. G. Chaudhary, P. B. Chouke, S. Yerpudeb, A. Mondal, V. N. Sonkusared, A. R. Raib, H. D. Junejad, *Mater. Sci. Eng. C* **2019**, *99*, 783–793.
- [23] Y. Guo, Q. Sun, F. G. Wu, Y. Dai, X. Chen, *Adv. Mater.* **2021**, *33*, 2007356.
- [24] C. N. Mulligan, *Environ. Pollut.* **2005**, *133*, 183–198.
- [25] Y. T. Zhang, W. Wei, J. Sun, Q. Xu, B. J. Ni, *Environ. Sci. Technol.* **2020**, *54*, 9662–9671.
- [26] N. Shreyash, S. Bajpai, M. A. Khan, Y. Vijay, S. K. Tiwary, M. Sonker, *ACS Appl. Nano Mater.* **2021**, *4*, 11428–11457.
- [27] K. M. Nelson, J. L. Dahlin, J. Bisson, J. Grahams, G. F. Pauli, M. A. Walters, *J. Med. Chem.* **2017**, *60*, 1620–1637.
- [28] V. Conman, D. C. Vodnar, *J. Sci. Food Agric.* **2020**, *100*, 483–499.

- [29] T. Farkhondeh, S. Samarghandian, A. M. P. Shahri, M. Sedaghat, *J. Cell. Physiol.* **2019**, *234*, 16853–16965.
- [30] T. Esatbeyoglu, P. Huebbe, I. M. A. Ernst, D. Chin, A. E. Wagner, G. Rimbach, *Angew. Chem. Int. Ed.* **2012**, *51*, 5308–5332; *Angew. Chem.* **2012**, *124*, 5402–5427.
- [31] C. Magnani, V. L. B. Issac, M. A. Correa, H. R. N. Salgado, *Anal. Methods* **2014**, *6*, 3203–3210.
- [32] X. X. Yang, C. M. Li, C. Z. Huang, *Nanoscale* **2016**, *8*, 3040–3048.
- [33] N. G. Gogoi, J. G. Handique, *J. Chem. Sci.* **2019**, *131*, 1–11.
- [34] A. Soto-Quintero, N. Guarrotxena, O. Gracia, I. Quijada-Garrido, *Sci. Rep.* **2019**, *9*, 18187.
- [35] A. Gupta, S. M. Briffa, S. Swingler, H. Gibson, V. Kannappan, G. Adamus, M. Kowalczyk, C. Martin, I. Radecka, *Biomacromolecules* **2020**, *5*, 1802–1811.
- [36] S. Roy, R. Priyadarshi, P. Ezati, J. W. Rhim, *Food Chem.* **2021**, *375*, 131885.
- [37] G. Cui, W. Su, M. Tan, *Compr. Rev. Food Sci. Food Saf.* **2022**, *21*, 2002–2031.
- [38] A. Tomak, S. Cesmeli, B. D. Hanoglu, D. Winkler, C. O. Karakus, *Nanotoxicology* **2021**, *15*, 1331–1357.
- [39] A. Sahraei, F. Mohammadi, R. Boukherroub, S. Szunertis, *Langmuir* **2020**, *36*, 10321–10330.
- [40] S. Ghosh, J. Dey, *J. Phys. Chem. B* **2015**, *119*, 7804–7815.
- [41] C. A. Rouzer, L. J. Marnett, *Chem. Rev.* **2020**, *120*, 7592–7641.
- [42] K. N. Thakkar, S. S. Mhatre, R. Y. Parikh, *Nanomed. Nanotechnol. Biol. Med.* **2010**, *6*, 257–262.
- [43] A. D. Verma, N. Jain, S. K. Singha, M. A. Quraishi, I. Sinha, *J. Chem. Sci.* **2016**, *128*, 1871.
- [44] P. K. Sahu, *Eur. J. Med. Chem.* **2016**, *121*, 510.
- [45] A. Baral, L. Satish, D. P. Das, H. Sahood, M. K. Ghosh, *New J. Chem.* **2017**, *41*, 8130–8139.
- [46] L. Satish, S. Rana, M. Arakha, L. Rout, B. Ekka, S. Jha, P. Dash, H. Sahoo, *Spectrosc. Lett.* **2016**, *49*, 383–390.
- [47] M. I. Gadallah, H. R. H. Ali, H. F. Askal, G. A. Saleh, *Spectrochim. Acta Part A* **2021**, *246*, 119005.
- [48] B. K. Paul, K. Bhattacharjee, S. Bose, N. A. Guchhait, *Phys. Chem. Chem. Phys.* **2012**, *14*, 15482–15493.
- [49] A. Sułkowska, *J. Mol. Struct.* **2002**, *614*, 227–232.
- [50] A. Mittal, S. Gandhi, I. Roy, *Sci. Rep.* **2022**, *12*, 10331.
- [51] W. Villarreal, L. Colina-Vegas, G. Visbal, O. Corona, R. S. Correa, J. Ellena, M. R. Cominetti, A. A. Batista, M. Navarro, *Inorg. Chem.* **2017**, *56*, 3781–3793.
- [52] X. Zhao, R. Liu, Z. Chi, Y. Teng, P. Qin, *J. Phys. Chem. B* **2010**, *114*, 5625–5631.
- [53] J. Liu, J. N. Tian, J. Zhang, Z. Hu, X. Chen, *Anal. Bioanal. Chem.* **2003**, *376*, 864–867.
- [54] D. P. Tamboli, D. S. Lee, *J. Hazard. Mater.* **2013**, *260*, 878–884.
- [55] E. A. Masoud, A. M. Al-Hajry, A. Al-Marrani, *Int. J. Curr. Microbiol. Appl. Sci.* **2016**, *5*, 226.
- [56] A. K. Potbhare, M. S. Umekar, P. B. Chouke, M. B. Bagade, S. K. Tarik Aziz, A. A. Abdala, R. G. Chaudhary, *Mater. Today: Proc.* **2020**, *29*, 815–821.
- [57] P. B. Chouke, A. K. Potbhare, N. P. Meshram, M. M. Rai, K. M. Dadure, K. Chaudhary, A. R. Rai, M. F. Desimone, R. G. Chaudhary, D. T. Meshram, *ACS Omega* **2022**, *7*, 6869–6884.
- [58] W. Brand-Williams, M. E. Cuvelier, C. Berset, *Food Sci. Technol.* **1995**, *28*, 25–30.
- [59] P. Singla, V. Luxami, K. Paul, *Eur. J. Med. Chem.* **2016**, *117*, 59–69.
- [60] P. K. Sahu, P. K. Sahu, S. K. Gupta, D. Thavaselvam, D. D. Agarwal, *Eur. J. Med. Chem.* **2012**, *54*, 366–378.

Submitted: October 13, 2022

Accepted: December 2, 2022

RESEARCH ARTICLE



*N. Gandha Gogoi, Prof. Dr. P. Dutta,
Dr. J. Saikia*, Prof. Dr. J. G.
Handique**

1 – 9

**Antioxidant, Antibacterial, and
BSA Binding Properties of
Curcumin Caffeate Capped Silver
Nanoparticles Prepared by
Greener Method**



Curcumin caffeate (CCaf) polyphenol acts as an effective capping and reducing group in preparing stabilized AgNPs in aqueous medium and at room conditions. The process is eco-friendly owing to the no-toxicity of

CCaf and use of external chemical reductants. The AgNPs are found to have antioxidant, and antibacterial activity against ESKAPE bacterial pathogens and effective BSA binding interactions.

See discussions, stats, and author profiles for this publication at: <https://www.researchgate.net/publication/366498200>

Antioxidant, Antibacterial, and BSA Binding Properties of Curcumin Caffeate Capped Silver Nanoparticles Prepared by Greener Method

Article in *ChemistrySelect* · December 2022

DOI: 10.1002/slct.202203989

CITATIONS

0

READS

127

4 authors, including:



Nishi Gandha Gogoi

MDKG College

6 PUBLICATIONS 8 CITATIONS

[SEE PROFILE](#)



Pankaj Dutta

Dibrugarh University

32 PUBLICATIONS 221 CITATIONS

[SEE PROFILE](#)

Antioxidant, Antibacterial, and BSA Binding Properties of Curcumin Caffeate Capped Silver Nanoparticles Prepared by Greener Method

Nishi Gandha Gogoi,^[a] Pankaj Dutta,^[b] Jiban Saikia,^{*[a]} and Jyotirekha G. Handique^{*[a]}

A green method of silver nanoparticle (AgNP) preparation using curcumin caffeate (CCaf) as stabilizing/capping and reducing group is reported here. CCaf is prepared through esterification of curcumin and caffeic acid in presence of *p*-toluene sulphonic acid as catalyst. CCaf facilitates production of AgNPs in aqueous medium and room temperature without any external reducing agents. The antioxidant, antibacterial and BSA binding interactions of these CCafAgNPs are evaluated. The antioxidant activity and the corresponding IC₅₀ value for the CCafAgNPs is found to be comparable with ascorbic acid

taken as standard antioxidant for the study. The results of bactericidal screening of CCafAgNPs are better compared to CCaf capping group and found to exhibit broad spectrum antibacterial property against Gram-positive and Gram-negative bacterial pathogens. In presence of CCafAgNPs the absorption spectra of BSA showed changes with increase in intensity around 280 nm of native BSA peak and appearance of a new band around 320 nm, indicating the possible binding interactions between BSA and CCafAgNPs.

Introduction

Nanoparticles are gaining utmost attention in the 21st century for their diverse applications in catalytic, optoelectronics, electrical, biomedicine and pharmaceutical fields.^[1–4] Silver nanoparticles (AgNPs) have beneficial properties and applications in biotechnology and medicinal ground as antioxidants, anti-inflammatory drugs, antibiotics, and biosensors, and hence are most intensively studied in the recent decades.^[5–8] The antibacterial and anti-inflammatory properties of AgNPs finds use in medicine to reduce or inhibit bacterial growth on human skin and medical equipment, burns and wounds, water treatment and textiles.^[9,10] Often, AgNPs have the tendency to agglomerate, resulting in increase in particle size and decrease in their surface energy and beneficial usability.^[11] AgNPs without a support/capping group is hard to recover and reuse. The morphology of the AgNPs including their shape and size and type of capping material used, is important in tuning the properties of AgNPs.^[12] Therefore, researchers are involved in extensive studies for developing new and improved synthesis methods for regulating the morphology of AgNPs.

Considering the environmental disadvantages of the conventional chemical and physical methods green methodologies

are developed in preparing AgNPs in recent times. Chemical reduction, laser synthesis, photo reduction, etc. are energy and time consuming and require strict preparation conditions.^[13–15] At the same time, some of these methods incorporate use of hazardous chemicals as hydrazines or borohydrides as reducing agents, and release environmentally contaminated byproducts.^[16,17] The production of AgNPs by toxic conditions is a critical concern and threat to the environment and so, replacement by safe and sustainable alternatives are gaining importance. Utilization of plant extracts and their components are gathering interests of the scientists as an easy, fast, economic, and environment sustainable technique for production of AgNPs.^[18–20]

Plant based components such as polyphenols, polymers and hydrogels are non-toxic and biodegradable and therefore, are explored and preferred as capping and reducing agents in preparation of metallic nanomaterials,^[21,22] over the synthetic polymers such as polyvinylchloride (PVC), polyacrylamides, polyurethanes (PU), and polyethylene glycols (PEGs), ionic surfactants such as sodium dodecyl sulphate (SDS) and non-ionic surfactants such as Brij, Tween, etc.^[23–26] Polyphenols such as curcumin and hydroxycinnamic acids possess no toxicity issues to human health and so their antioxidant, anti-bacterial, anti-cancer, anti-inflammatory, and anti-alzheimer activities are explored over many years.^[27–29] Curcumin, a natural yellow-orange compound, extracted from the roots of *Curcuma longa* rhizome and is used in medicinal applications by oriental cultures.^[28] Hydroxycinnamic acids includes caffeic, coumaric, ferulic, and sinapic acids which are mostly found in plants and plant products such as cereals, legumes, fruits, vegetables, and oilseeds. Caffeic acid is mainly found in plants and their products such as coffee, tea, wine, etc.^[30] In addition to the proven medicinal properties, curcumin and its derivatives have been used as reducing and capping agent in AgNP production.^[31–34] These curcumin capped AgNPs are reported to

[a] N. Gandha Gogoi, Dr. J. Saikia, Prof. Dr. J. G. Handique
Department of Chemistry
Dibrugarh University
786004 Dibrugarh, Assam, India
E-mail: jghandique@dibru.ac.in
ngogoi28@gmail.com

[b] Prof. Dr. P. Dutta
Department of Physics
Dibrugarh University
786004 Dibrugarh, Assam, India


 Supporting information for this article is available on the WWW under <https://doi.org/10.1002/slct.202203989>

exhibit antimicrobial and antioxidant properties that can be exploited in designing food packaging and wound healing material.^[35,36]

In the course of using nanoparticles for medical purposes, the nanoparticles are applied/released to the protein surfaces for binding and delivering at the target site.^[37] Many forces such as vander Waals forces, hydrogen bonding, and hydrophobic interactions are involved in the process of adsorption of NPs on the surface of protein and forming a layer.^[38] It is important to understand the nature of interactions that develops between the protein and NPs for exploring the effects of binding of NPs on structure and stability of protein and safe drug delivery at the expected target site.^[39] For this purpose, bovine serum albumin (BSA) is mostly employed. Serum albumins are abundantly available in blood plasma and are involved in transport of various exogenous and endogenous compounds.^[40] BSA has 583 amino acid residues and the secondary structure consists of mainly α helices and the remaining are β sheets, twists and coils. It has three domains I, II and III with two subdomains A and B each. There are two tryptophan (Trp124 and Trp 213) and phenylalanine (Phe) residues at the binding site.^[41]

To the best of our knowledge, curcumin caffeate capped AgNPs and the evaluation of their biomedical properties are not reported earlier. In this work, we synthesized curcumin caffeate derivative of curcumin and used it as reducing and capping agent in AgNPs production in aqueous medium and room conditions without use of any external mechanical applications. The antioxidant behaviour of AgNPs is measured by DPPH assay. Bactericidal property is screened for Gram-positive bacteria -Staphylococcus aureus, and Gram-negative bacteria – Escherichia coli, Klebsiella pneumoniae, Acinetobacter baumannii, and Pseudomonas aeruginosa. The drug-protein binding interaction between BSA and AgNPs is studied by UV-visible and fluorescence spectrophotometer.

Results and Discussion

Curcumin caffeate (CCaf) was prepared by Knoevenagel condensation between curcumin and caffeic acid. Briefly, curcumin (1 mM) and caffeic acid (2 mM) is dissolved in ethanol and refluxed for 6 hours in presence of para-toluene sulphonic acid (p-TSA) as catalyst. The reaction was monitored by recording thin layer chromatography (TLC) plates at different time intervals. The extra solvent was removed and the product was extracted, washed with aqueous base and acid solutions, filtered, dried in sodium sulphate and purified by column chromatography. The characterization of CCaf was done by using FT-IR, ^1H and ^{13}C NMR and LCMS spectrometric techniques. Furthermore, CCaf was used in easy and green preparation of AgNPs from AgNO_3 in aqueous medium and at room temperature (27°C). Most of the methods reported in literature often require high preparation temperature, long reaction time, external equipment or toxic reducing agents.^[42] In the present silver nanoformulation procedure, CCaf as capping and reducing complex completes the AgNPs production in safe and

simple operating eco-friendly conditions, consuming less (or no) energy and solvent and without producing waste.

The surface plasmon resonance (SPR) phenomenon of the synthesized AgNPs on CCaf as stabilizer was characterized by monitoring the absorbance spectrum at different time intervals in UV-visible spectral region. AgNPs are reported to yield a SPR absorption band in the visible region around 400 nm due to the resonance of their free electrons with the photons in that spectral region. Figure 1 depicts the absorption spectrum of CCafAgNPs recorded at different time intervals during the synthesis procedure. In the initial stages of synthesis, AgNO_3 dissociates releasing Ag^+ and NO_3^- ions in aqueous medium. The hydroxyl groups on CCaf encapsulate the silver ions when it was added to the reaction medium followed by reduction of Ag ions to give the CCafAgNPs. Physical changes observed in the colour from yellow to dark green indicate the formation of AgNPs, confirmed by a SPR band at 424 nm, reduced and stabilized by CCaf complex.

The sharp and intense distinct peaks XRD pattern shows the crystallinity of the AgNPs (Figure 2). The peaks at 38:18, 44:29, 64:43, and 77:48 are well indexed to the 111, 200, 220 and 311 planes of silver, respectively and are in good agreement with the face centered cubic (FCC) lattice structure Ag

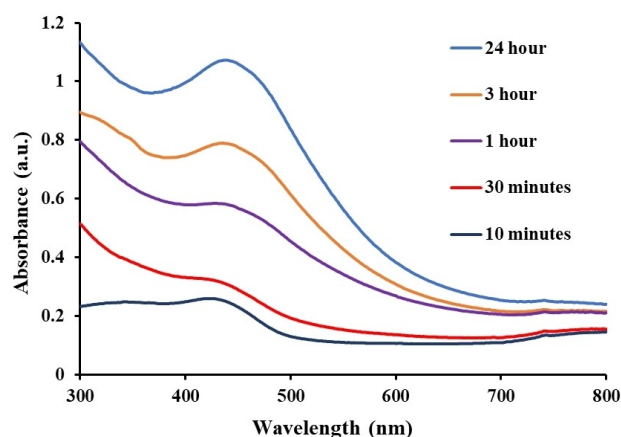


Figure 1. Absorption spectrum of CCaf-AgNPs at different time intervals.

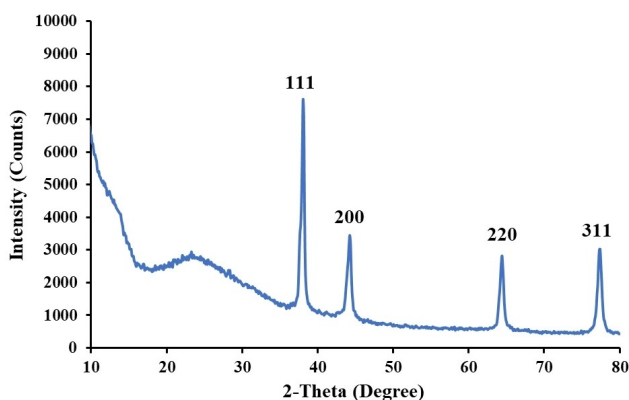


Figure 2. XRD pattern of CCafAgNPs.

(JCPDS silver file No. 04-0783).^[43] The relatively high intense signal is that of 111 Bragg's reflection and reveals its exposure in the structure. Presence of no other signals indicates the purity of sample. The elemental EDX profile shown in Figure 3, demonstrates a sharp signal of silver at 3 keV, confirming the major element in the NPs as silver. Along with silver, prominently distinguishable peaks of oxygen, carbon and chlorine are observed in the EDX pattern in the signal range of 0–0.5 keV. This confirms the presence of CCaf as capping agent on the surface of AgNPs that tends to prevent aggregation of AgNPs.

The morphology of the surface of AgNPs and their particle shape and size distribution are demonstrated by the SEM (Figure 3) and TEM results. High resolution TEM images showed that the AgNPs formed by CCaf are relatively spherical in shape. The crystallite size of CCafAgNPs estimated from Debye Scherrer's formula is 30 nm with interplanar spacing of 0.235 nm corresponding to the 111 plane (Figure 4a). The highly-dense AgNPs are homogeneously distributed. The selected area electron diffraction (SAED) pattern (Figure 4b) shows crystalline nature of AgNPs and spotty rings corresponds to the 111, 200, 220 and 311 planes, as observed in XRD profile.

Antioxidant activity

The free radicals and reactive oxygen species, generated from cellular oxidation are responsible for adverse cellular damage and chronic diseases. The reactive radical species as H_2O_2 , $\bullet\text{O}_2^-$ (superoxide anion), OH (hydroxyl radical), NO and $^1\text{O}_2$ (singlet oxygen) are responsible for causing damage at the cellular and tissue sites by injuring the peptides, nucleic acids, and lipids in inflammatory cells leading to chronic health conditions. Antioxidants are known to decelerate these devastating effects by neutralizing these free radicals and species.^[44] The antioxidant activity of CCafAgNPs is evaluated through DPPH assay shown in Figure 5. Ascorbic acid is used as a standard antioxidant. The antioxidant capacity of the CCafAgNPs is found to increase with its increasing concentration resulting in enhanced ability to scavenge DPPH radical. The IC_{50} values are calculated from the plot of % inhibition versus concentration

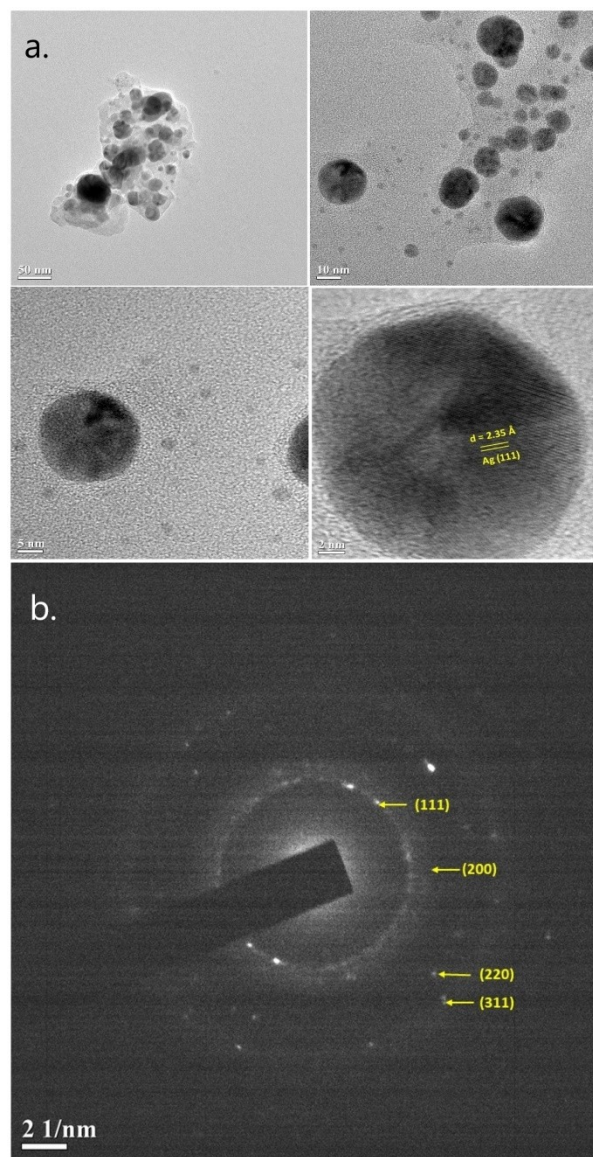


Figure 4. a. TEM images, and b. SAED pattern of CCafAgNPs.

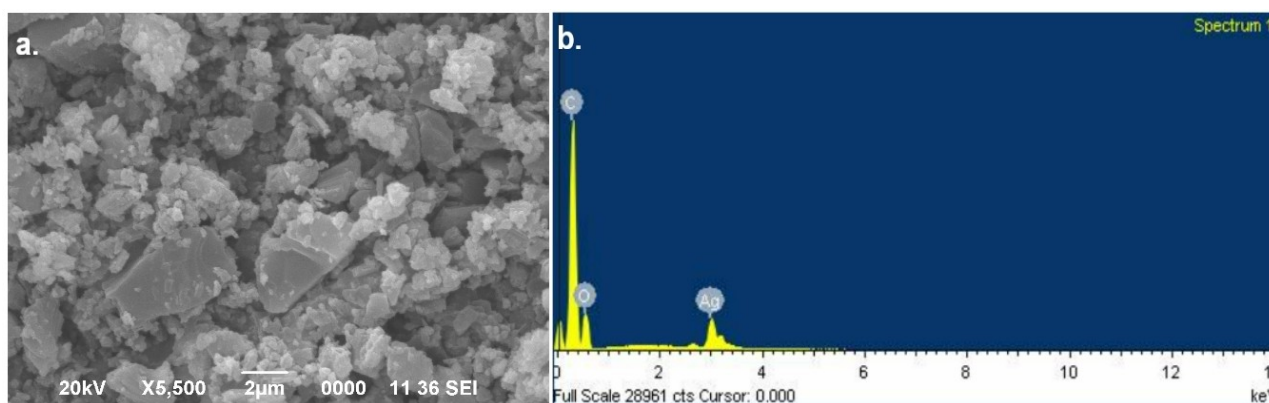


Figure 3. Scanning electron microscopy (SEM), and energy dispersive X-ray (EDX) analysis of CCafAgNPs.

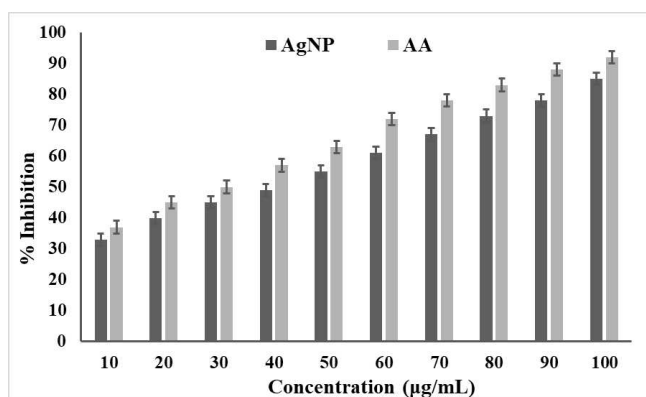


Figure 5. DPPH radical scavenging activity of CcAgAgNPs (AgNP) and ascorbic acid (AA) as standard antioxidant.

graph. Although antioxidant capacity of AgNPs is lower than ascorbic acid, but their IC_{50} values are quite comparable i.e., 57.13 $\mu\text{g/mL}$ for AgNPs, and 45.40 $\mu\text{g/mL}$ for ascorbic acid. The observed antioxidant behaviour of AgNPs is accounted for the presence of hydroxyl groups present on the capping group.

BSA binding study

UV-visible absorbance

The interaction of BSA and CcAgAgNPs is observed from the UV-visible absorption and steady state fluorescence spectra measurements. In absence of CcAgAgNPs, BSA shows two absorption peaks at 200–230 nm (corresponding to $\pi \rightarrow \pi^*$ transition of polypeptide chain) and 260–290 nm due to $n \rightarrow \pi^*$ transition of the Tyr/Trp chromophores.^[45] The intensity of the absorption peak of BSA around 280 nm is found to change in presence of CcAgAgNPs with the appearance of a new band around 320 nm, shown in figure 6. The intensity of the peak increases with increase in the concentration from 10–100 $\mu\text{g/mL}$ of AgNPs. The hypsochromic shift is due to formation of a ground state complex between BSA and CcAgAgNPs.^[46] Similar results of BSA and nanoparticles are reported in literature.^[47] These changes clearly indicate the interaction of BSA and CcAgAgNPs and change in the microenvironment near Trp, Tyr and Phe residues located in the binding cavity of BSA. The

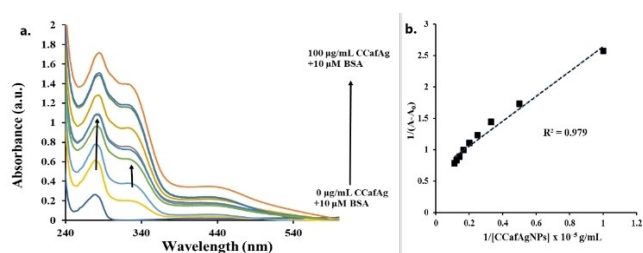


Figure 6. a. Absorption spectrum of BSA-CCafAgNPs binding interactions; b. Benesi-Hildebrand plot of $1/(A-A_0)$ versus $1/[CCafAgNPs]$.

nature of quenching of BSA in presence of AgNPs is static in this case,^[47] as indicated by the change of absorption spectra of BSA. The polar and hydrophobic interactions between the hydroxy groups and aromatic moieties of CCaf and polar and hydrophobic amino acid residues on BSA respectively, are responsible for the observed binding interactions. The binding constant, K_{app} of CCafAgNPs-BSA protein from absorbance spectrum is calculated from the Benesi-Hildebrand plot (equation 1) of $1/(A-A_0)$ versus $1/[CCafAgNPs]$ and found to be $3.52 \times 10^4 \text{ M}^{-1}$.

$$\frac{1}{(A-A_0)} = \frac{1}{(A_C-A_0)} + \frac{1}{K_{app}(A_C-A_0)} \times [CCafAgNPs] \quad (1)$$

where, A is the absorbance observed for BSA with different concentrations of ligand; A_0 is the blank absorbance of BSA; A_C is the maximum absorbance of BSA with ligand; K_{app} is the apparent binding constant. A graph of $1/(A_{obs}-A_0)$ versus $1/[CCafAgNPs]$ the ratio of intercept to slope of the linear fit plot gave the K_{app} of BSA and ligand.

Steady state fluorescence emission

The quenching of emission intensity of a fluorophore in presence of a complex occurs due to various molecular interactions such as molecular rearrangements, energy transfer, excited state reactions, collisions among molecules (dynamic quenching) or formation of ground state complex (static quenching).^[48] BSA shows fluorescence for the presence of three intrinsic fluorophores in their structure- Phe, Tyr and Trp. Trp is considered as the main contributor of showing fluorescence in BSA as Phe and Tyr are opted out for low fluorescence quantum yield and high fluorescence quenching in presence of amino/carboxyl group, respectively.^[49] The fluorescence quenching is important in establishing the binding interaction of BSA in presence of ligands as Trp residue is highly responsive to the minor change in hydrophobicity or polarity in its surrounding.^[50] It is observed that the fluorescence intensity of BSA diminishes with increase in concentration of ligands. Figure 7 shows the fluorescence emission spectra of CcAgAgNPs and BSA and the corresponding Benesi-Hildebrand plot of $1/(F_0-F)$ versus $1/[CCafAgNPs]$ for BSA where F_0 is the fluorescence intensity of BSA in absence of ligand and F is the fluorescence intensity in presence of ligand. The K_{app} value of BSA-CCafAgNPs binding from fluorescence spectra is found to be $9.02 \times 10^4 \text{ M}^{-1}$.

Stern-Volmer equation (equation 2) explains the nature of mechanism of protein-ligand quenching i.e., whether it is static quenching or dynamic quenching.

$$\frac{F_0}{F} < C \Rightarrow K_{sv} [CCafAgNPs] + 1 \quad (2)$$

$$K_{sv} = K_q \tau_0 \quad (3)$$

where, F and F_0 are the fluorescence intensity of serum albumins in the presence and absence of CcAgAgNPs as

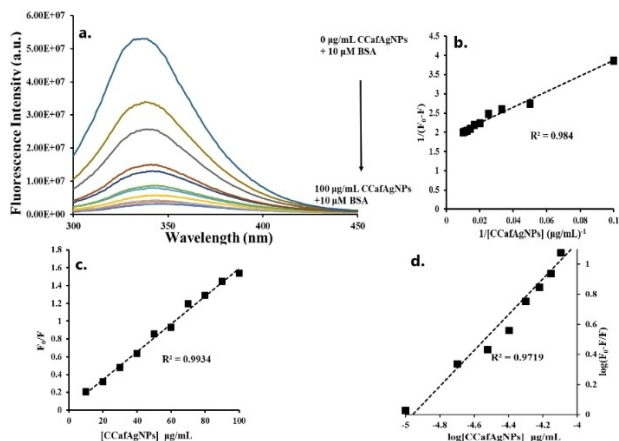


Figure 7. a. Fluorescence emission spectrum of BSA-CCafAgNPs with increasing concentration of CCafAgNPs (0–100 µg/mL); b. Benesi-Hildebrand plot of $1/(F_0 - F)$ versus $1/[CCafAgNPs]$; c. Stern-Volmer plot of F_0/F versus $[CCafAgNPs]$; d. double logarithmic modified Stern-Volmer plot.

quencher and K_{SV} is Stern-Volmer constant. The quenching constant, K_q is the ratio of K_{SV} and τ_0 (average lifetime of BSA; 10^{-8} s for BSA).^[51] The slope of the linear Stern-Volmer plot of F_0/F vs. $[CCafAgNPs]$ of BSA is equal to the value of K_{SV} ($0.156 \times 10^5 M^{-1}$). The calculated K_q value is $1.56 \times 10^{12} M^{-1} s^{-1}$ and is greater than collision quenching constant $2.0 \times 10^{10} M^{-1} s^{-1}$.^[52] This confirms quenching mechanism to be static quenching for formation of ground state complex between BSA and CCafAgNPs. The ground state complex formed is stabilised by non-covalent interactions as electrostatic, van der Waals or hydrophobic forces and formation of hydrogen bonds.^[53]

The number of binding sites between BSA and CCafAgNPs is given by modified Stern-Volmer electrostatic equation (equation 3)

$$\log\left(F^0 - \frac{F}{F}\right) = n \log[CCafAgNPs] + \log K_{app} \quad (4)$$

n is the number of binding sites between CCafAgNPs and BSA calculated from the linear plot of $\log(F_0 - F)/F$ versus $\log[CCafAgNPs]$. CCafAgNPs are found to uniquely bind to BSA ($n = 1.191$). The spectroscopic results from fluorescence and UV-visible is found to be in good agreement with formation of

ground state complex and can be concluded from the observed changes of both the spectroscopic analysis.

Antibacterial activity

The bactericidal property of CCafAgNPs, CCaf and curcumin is screened against both Gram positive bacteria – *S. aureus* ATCC 29213, and Gram-negative bacteria – *E. coli* ATCC 25922, *K. pneumoniae* BAA 1705, *A. baumannii* BAA 1605, and *P. aeruginosa* ATCC 27853 by evaluating the minimum inhibitory concentration (MIC) values of AgNPs by microbroth dilution assay. Levofloxacin is used as a standard antibiotic. CCafAgNPs are found to exhibit broad-spectrum antibacterial activity against these bacterial pathogens and are more effective than curcumin and CCaf (capping agent), as shown in Table 1, due to the presence of Ag metal. The positive charge on CCafAgNPs is attracted by the negative charge on bacterial cell wall leading to the releasing of silver ions through pore formation inside the bacterial cell membranes. Inside the membrane, the affinity of silver ions for sulphur and phosphorus containing macromolecules results in disruption of ATP production and DNA replication. AgNPs also causes oxidative stress inside bacterial cell membrane by triggering the generation of free radicals ultimately leading to cell death.^[54–57] The combinatorial action of the AgNPs on bacterial cell accounts for their inhibitory effect as antibacterial compounds.

Conclusion

In this work, AgNPs capped and reduced by curcumin caffeate (CCaf) polyphenol is prepared for the first time by cost-effective and greener method. The stabilized AgNPs are characterized by XRD, SEM-EDX and TEM analytical techniques. The fabricated nanomaterial is found to have a face centred cubic lattice and average size of each particle is found to be 30 nm. The biological properties of CCafAgNPs are evaluated and found to have effective antioxidant, and antibacterial properties which may be used further in pharmaceutical fields, or in sterilization procedures. CCafAgNPs are found to be effective against both gram-positive and gram-negative bacterial pathogens (compared to curcumin and CCaf) which makes CCafAgNPs eligible to be used in food packaging materials as sensors for microbial contamination. The BSA-nanoparticle interactions have also been studied by UV-visible and fluorescence emission spectroscopic methods. The BSA-CCafAgNPs binding interaction study may provide initial insight in nanobiotechnology and designing

Table 1. Minimum Inhibitory Concentration (MIC in µg/ml) of CCafAgNPs, CCaf and curcumin on tested bacterial pathogens (triplicate studies). DMSO is used as the negative control and Levofloxacin as the positive control. ‘-’ indicate no activity.

Drug	Minimum inhibitory concentration (MIC in µg/ml)				
	<i>E. coli</i> ATCC 25922	<i>S. aureus</i> ATCC 29213	<i>K. pneumoniae</i> BAA 1705	<i>A. baumannii</i> BAA 1605	<i>P. aeruginosa</i> ATCC 27853
CCafAgNPs	64	64	> 64	64	64
CCaf	> 64	64	> 64	> 64	> 64
Curcumin	> 64	> 64	> 64	> 64	> 64
Levofloxacin (Std)	0.0156	0.25	64	8	1
DMSO	-	-	-	-	-

new drugs and further detailed study in this domain are needed.

Experimental Section

Methods

UV-visible absorption and Fluorescence spectrophotometry

The SPR phenomenon of AgNPs resulting from reduction of Ag⁺ ions by CCaf are monitored by Hitachi U-3900H UV-visible spectrophotometer and HORIBA Fluoromax-4 fluorescence spectrophotometer. The analysis is performed using distilled water as reference in quartz cuvettes and diluting 1 mL of AgNPs suspension 4 mL of distilled water.

Fourier transform infrared spectra (FTIR)

FTIR spectra is recorded in the range of 400–4000 nm with a Shimadzu IRPrestige-21 FTIR spectrophotometer on KBr palletes.

Nuclear magnetic resonance (NMR)

¹H and ¹³C NMR spectra are recorded by a Bruker Advance II spectrophotometer at 400 MHz and 100 MHz, respectively in DMSO-d₆ solvent and TMS as internal standard.

Molecular mass spectra

Molecular mass of CCaf is measured by a Ultimate 3000/TSQ Endura liquid chromatograph mass spectrometer (LCMS).

Powder X-ray diffraction (XRD)

XRD pattern is recorded with a Bruker AXS D8 Focus X-ray diffractometer by irradiating monochromatic Cu-Kα (1.541 Å radiation).

Transmission electron microscopy (TEM)

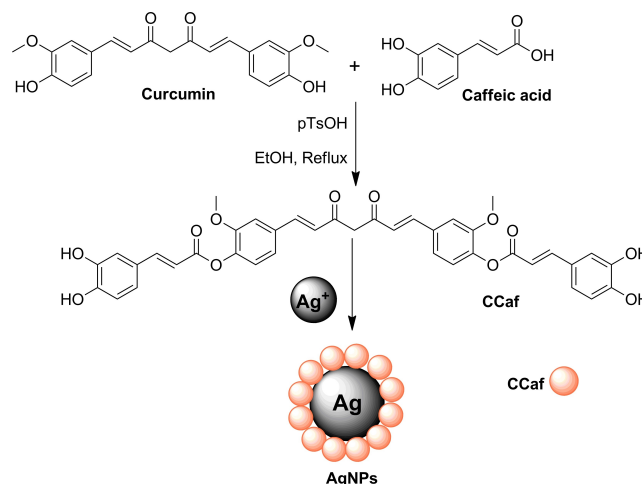
Transmission electron Microscopy (TEM) and selected area diffraction (SAED) analysis of stabilized AgNPs is performed with a JEM-100 CX II transmission electron microscope equipped operating at 20–100 KV in 20 KV steps having high resolution CCD camera from 3 Å to 1.4 Å.

Scanning electron microscopy (SEM)

Scanning electron microscopy (SEM) and energy dispersive X-ray (EDX) spectra is recorded in JEOL/JSM 6390LV scanning electron microscope.

Synthesis of curcumin caffeate (CCaf)

Curcumin caffeate is prepared by the method reported earlier. Briefly, a mixture of curcumin (1 mM) and caffeic acid (2 mM) in ethanol is refluxed for 6 h at 60 °C in presence of p-TsOH and under nitrogen atmosphere with constant stirring. The completion of the reaction is monitored by examining TLC. The solvent is removed under reduced pressure using rotatory evaporator, and the product so formed is purified by column chromatography (Scheme 1).



Scheme 1. Preparation of CCaf from curcumin and caffeic acid and AgNPs reduced/capped by CCaf.

Characterization is done by FTIR, ¹H and ¹³C NMR and LCMS analysis.

(2E,2'E)-((1E,6E)-3,5-dioxohepta-1,6-diene-1,7-diyl)bis(2-methoxy-4,1-phenylene)bis(3-(3,4-dihydroxyphenyl)acrylate) (CCaf)

Light orange solid. Yield: 0.486 g (70.2%). ¹H NMR (400 MHz, DMSO-d₆) δ 7.50 (d, J = 12 Hz, =C–H), 7.26 (s, Ar–H), 7.12 (dd, J = 4 Hz, 4 Hz, Ar–H), 6.80 (d, J = 12 Hz, Ar–H), 6.71 (d, J = 16 Hz, =C–H), 6.63 (m, Ar–H), 6.58 (m, Ar–H), 6.40 (d, J = 16 Hz, =C–H), 6.05 (s, Ar–H), 5.84 (s, Ar–OH), 4.11 (s, –CH₂), 3.79 (m, –OCH₃); ¹³C NMR (100 MHz, DMSO-d₆) δ 183.08 (–C=O), 168.56 (–O–C=O), 149.38 (–C–OCH₃), 147.52 (–C–OCH₃), 145.54 (–C–OH), 140.36 (Ar–C), 130.53 (Ar–C), 128.69 (Ar–C), 126.84 (C=), 125.35 (–C=), 123.02 (Ar–C–O–C=O), 121.16 (–C=), 116.00 (Ar–C), 111.32 (Ar–C), 108.50 (Ar–C), 102.85 (Ar–C), 101.48 (Ar–C), 55.43 (–OCH₃), 51.75 (–CH₂); LCMS (m/z): 690.44 [M–2H]⁺ (Calculated M⁺ = 692.19).

Preparation of CCaf stabilized silver nanoparticles (green synthesis)

To a 1 mM aqueous silver nitrate (AgNO₃) solution (10 mL) at ambient temperature, 0.1 mM of CCaf is added. The reaction mixture turns brown colour, indicating the start of reduction process of Ag⁺ ions and development of AgNPs. The progress of the process of formation of AgNPs is monitored by UV-visible spectrophotometer. The mixture is centrifuged, washed with ethanol/water and dried to obtain the stabilized AgNPs (Scheme 1). The in-vitro antioxidant and antibacterial properties, and BSA -drug binding study of these CCafAgNPs are evaluated.

Antioxidant activity

The antioxidant property of CCaf-AgNPs is measured by DPPH-radical scavenging assay following the method described by Brand-Williams et al. with some modifications.^[58] AgNPs solution of concentrations 10–100 µg/mL in distilled water are prepared and mixed with 100 µM methanolic solution of DPPH. The reaction mixture is kept in the dark at room temperature for 30 minutes.

The absorbance of the reaction mixture is measured by UV-visible spectrophotometer at 517 nm in parallel with a reagent blank. The percent inhibitions of DPPH• by the antioxidants are measured by the bleaching of the purple colour of DPPH. The % inhibition is calculated as

$$\% \text{ DPPH} \cdot \text{inhibition} = ((A_b - A_e)/A_b) \times 100 \% \quad (5)$$

where, A_b is the absorbance of the blank reagent and A_e is the absorbance of the reaction mixture. Ascorbic acid is used as a standard. The results are shown as percentage (%) inhibition versus the concentrations CCafAgNPs.

BSA binding study

The BSA binding interactions with CCafAgNPs is studied UV-visible and fluorescence spectrophotometer by the change in absorption or emission spectra of BSA^[59] in presence of increasing concentrations of CCafAgNPs as ligand (10–100 µg/mL). The reaction mixture consists of 2 mL of BSA (10 µM) in phosphate buffer solution (PBS, pH 7.4), 0.5 mL of PBS and 0.5 mL of CCafAgNPs solution. The mixture is incubated at 37°C for 30 minutes before recording spectroscopic data. The binding constant (K_{app}) is evaluated from absorption data by Benesi-Hindelbrand equation (equation 6).

$$1/(A - A_0) = 1/(A_C - A_0) + 1/K_{app} (A_C - A_0) [\text{ligand}] \quad (6)$$

where, A is the absorbance observed for BSA with different concentrations of ligand; A_0 is the blank absorbance of BSA; A_C is the maximum absorbance of BSA with ligand; K_{app} is the apparent binding constant. A graph of $1/(A_{obs} - A_0)$ versus $1/[CCafAgNPs]$ and $1/(F_0 - F)$ versus $1/[CCafAgNPs]$ and the ratio of intercept to slope of the linear fit plot gave the K_{app} of BSA and ligand.

Antibacterial activity

The bactericidal property of CCafAgNPs is screened for ESKAPE pathogen panel- *Escherichia coli* ATCC 25922, *Staphylococcus aureus* ATCC 29213, *Klebsiella pneumoniae* BAA 1705, *Acinetobacter baumannii* BAA 1605, and *Pseudomonas aeruginosa* ATCC 27853 by microbroth dilution method.^[60] The results are expressed in terms of minimum inhibitory concentration (MIC) values in µg/mL. AgNPs of different concentrations (0–64 µg/mL) in DMSO is taken in different wells. Bacteria culture, grown in 5% Muller-Hinton broth for 18 h are rinsed with sterile phosphate buffer solution twice and diluted to $\sim 5 \times 10^5$ CFU/mL. Levofloxacin is used as standard antibiotic.

Supporting Information Summary

The spectroscopic data of the capping agent CCaf is included in the supplementary information.

Acknowledgements

We are grateful to the UGC, New-Delhi for Special Assistance Program (SAP-DRS) and Department of Science and Technology (DST), Govt. of India, for financial assistance under DST-FIST programme to the Department of Chemistry, Dibrugarh Univer-

sity. N. G. G. acknowledges DURF, Dibrugarh University for financial assistance. We acknowledge SAIC Tezpur University for SEM, EDX and XRD analysis, SAIF NEHU, Shillong for TEM analysis, and CDRI Lucknow for antibacterial screening tests.

Conflict of Interest

The authors declare no conflict of interest.

Data Availability Statement

The data that support the findings of this study are available from the corresponding author upon reasonable request.

Keywords: Antioxidant · Antibacterial · BSA binding · Curcumin caffeate · Silver nanoparticles

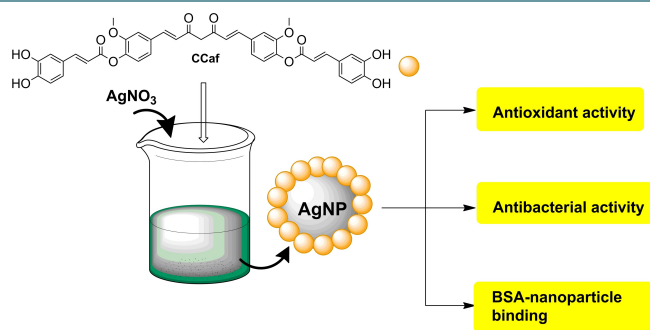
- [1] H. Barani, M. N. Boroumand, S. Rafiei, *Fibers Polym.* **2017**, *18*, 658–665.
- [2] Z. Zhang, W. Shen, J. Xue, Y. Liu, P. Yan, J. Liu, J. Tang, *Nanoscale Res. Lett.* **2018**, *13*, 54–72.
- [3] J. Zhang, S. Li, *Int. J. Environ. Anal. Chem.* **2019**, *101*, 1–23.
- [4] V. Vorobyova, G. Vasyliov, M. Skiba, *Appl. Nanosci.* **2020**, *10*, 4523–4534.
- [5] A. K. Potbhare, P. B. Chouke, A. Mondal, R. U. Thakare, S. Mondal, R. G. Chaudhary, A. R. Rai, *Mater. Today: Proc.* **2020**, *29*, 939–945.
- [6] A. K. Keshari, R. Srivastava, P. Singh, V. B. Yadav, G. Nath, *J. Ayurveda Integr. Med.* **2020**, *11*, 37–44.
- [7] M. Alavi, R. S. Varma, *Cellulose* **2021**, *28*, 8295–8311.
- [8] Z. Li, W. Ma, I. Ali, H. Zhao, D. Wang, J. Qiu, *ACS Omega* **2020**, *5*, 32632–32640.
- [9] S. Islam, B. S. Butola, A. Kumar, *Int. J. Biol. Macromol.* **2020**, *152*, 1135–1145.
- [10] K. Kalantari, E. Mostafavi, A. M. Affi, Z. Izadiyan, H. Jahangirian, R. Rafiee-Moghaddam, T. J. Webster, *Nanoscale* **2020**, *12*, 2268–2291.
- [11] X. Li, J. J. Lenhart, H. W. Walker, *Langmuir* **2012**, *28*, 1095–1104.
- [12] V. Bansal, V. Li, A. P. O'Mullane, S. K. Bhargava, *CrystEngComm* **2010**, *12*, 4280–4286.
- [13] S. Agnihotri, S. Mukherji, S. Mukherji, *RSC Adv.* **2014**, *4*, 3974–3983.
- [14] J. Kwon, J. Yeo, S. Hong, Y. D. Suh, H. Lee, J. Choi, S. S. Lee, S. H. Ko, *Energy Technol.* **2016**, *4*, 271–277.
- [15] H. Wang, X. Qiao, J. Chen, S. Ding, *Colloids Surf. A* **2005**, *256*, 111–115.
- [16] V. Gurusamy, R. Krishnamoorthy, B. Gopal, V. Veeraravagan, P. Neelamegam, *Inorg. Nano-Met. Chem.* **2017**, *47*, 761–767.
- [17] K. Mavani, M. Shah, *Int. J. Eng. Res. Technol.* **2013**, *2*, 1–5.
- [18] S. Ansar, H. Tabassum, N. S. M. Aladwan, M. N. Ali, B. Almaarik, S. AlMahrouqi, M. Abudawood, N. Banu, R. Alsubki, *Sci. Rep.* **2020**, *10*, 18564.
- [19] S. Jadoun, R. Arif, N. K. Jangid, R. K. Mehta, *Environ. Chem. Lett.* **2021**, *19*, 355–374.
- [20] C. Vanlalveni, S. Lallianrawna, A. Biswas, M. Selvaraj, B. Changmai, S. L. Rokhum, *RSC Adv.* **2021**, *11*, 2804–2837.
- [21] P. B. Chouke, A. K. Potbhare, K. M. Dadure, A. J. Mungole, N. P. Meshram, R. R. Chaudhary, A. R. Rai, R. G. Chaudhary, *Mater. Today: Proc.* **2020**, *29*, 720–725.
- [22] A. K. Potbhare, R. G. Chaudhary, P. B. Chouke, S. Yerpudeb, A. Mondal, V. N. Sonkusared, A. R. Raib, H. D. Junejad, *Mater. Sci. Eng. C* **2019**, *99*, 783–793.
- [23] Y. Guo, Q. Sun, F. G. Wu, Y. Dai, X. Chen, *Adv. Mater.* **2021**, *33*, 2007356.
- [24] C. N. Mulligan, *Environ. Pollut.* **2005**, *133*, 183–198.
- [25] Y. T. Zhang, W. Wei, J. Sun, Q. Xu, B. J. Ni, *Environ. Sci. Technol.* **2020**, *54*, 9662–9671.
- [26] N. Shreyash, S. Bajpai, M. A. Khan, Y. Vijay, S. K. Tiwary, M. Sonker, *ACS Appl. Nano Mater.* **2021**, *4*, 11428–11457.
- [27] K. M. Nelson, J. L. Dahlin, J. Bisson, J. Grahams, G. F. Pauli, M. A. Walters, *J. Med. Chem.* **2017**, *60*, 1620–1637.
- [28] V. Conman, D. C. Vodnar, *J. Sci. Food Agric.* **2020**, *100*, 483–499.

- [29] T. Farkhondeh, S. Samarghandian, A. M. P. Shahri, M. Sedaghat, *J. Cell. Physiol.* **2019**, *234*, 16853–16965.
- [30] T. Esatbeyoglu, P. Huebbe, I. M. A. Ernst, D. Chin, A. E. Wagner, G. Rimbach, *Angew. Chem. Int. Ed.* **2012**, *51*, 5308–5332; *Angew. Chem.* **2012**, *124*, 5402–5427.
- [31] C. Magnani, V. L. B. Issac, M. A. Correa, H. R. N. Salgado, *Anal. Methods* **2014**, *6*, 3203–3210.
- [32] X. X. Yang, C. M. Li, C. Z. Huang, *Nanoscale* **2016**, *8*, 3040–3048.
- [33] N. G. Gogoi, J. G. Handique, *J. Chem. Sci.* **2019**, *131*, 1–11.
- [34] A. Soto-Quintero, N. Guarrotxena, O. Gracia, I. Quijada-Garrido, *Sci. Rep.* **2019**, *9*, 18187.
- [35] A. Gupta, S. M. Briffa, S. Swingler, H. Gibson, V. Kannappan, G. Adamus, M. Kowalczyk, C. Martin, I. Radecka, *Biomacromolecules* **2020**, *5*, 1802–1811.
- [36] S. Roy, R. Priyadarshi, P. Ezati, J. W. Rhim, *Food Chem.* **2021**, *375*, 131885.
- [37] G. Cui, W. Su, M. Tan, *Compr. Rev. Food Sci. Food Saf.* **2022**, *21*, 2002–2031.
- [38] A. Tomak, S. Cesmeli, B. D. Hanoglu, D. Winkler, C. O. Karakus, *Nanotoxicology* **2021**, *15*, 1331–1357.
- [39] A. Sahraei, F. Mohammadi, R. Boukherroub, S. Szunertis, *Langmuir* **2020**, *36*, 10321–10330.
- [40] S. Ghosh, J. Dey, *J. Phys. Chem. B* **2015**, *119*, 7804–7815.
- [41] C. A. Rouzer, L. J. Marnett, *Chem. Rev.* **2020**, *120*, 7592–7641.
- [42] K. N. Thakkar, S. S. Mhatre, R. Y. Parikh, *Nanomed. Nanotechnol. Biol. Med.* **2010**, *6*, 257–262.
- [43] A. D. Verma, N. Jain, S. K. Singha, M. A. Quraishi, I. Sinha, *J. Chem. Sci.* **2016**, *128*, 1871.
- [44] P. K. Sahu, *Eur. J. Med. Chem.* **2016**, *121*, 510.
- [45] A. Baral, L. Satish, D. P. Das, H. Sahood, M. K. Ghosh, *New J. Chem.* **2017**, *41*, 8130–8139.
- [46] L. Satish, S. Rana, M. Arakha, L. Rout, B. Ekka, S. Jha, P. Dash, H. Sahoo, *Spectrosc. Lett.* **2016**, *49*, 383–390.
- [47] M. I. Gadallah, H. R. H. Ali, H. F. Askal, G. A. Saleh, *Spectrochim. Acta Part A* **2021**, *246*, 119005.
- [48] B. K. Paul, K. Bhattacharjee, S. Bose, N. A. Guchhait, *Phys. Chem. Chem. Phys.* **2012**, *14*, 15482–15493.
- [49] A. Sułkowska, *J. Mol. Struct.* **2002**, *614*, 227–232.
- [50] A. Mittal, S. Gandhi, I. Roy, *Sci. Rep.* **2022**, *12*, 10331.
- [51] W. Villarreal, L. Colina-Vegas, G. Visbal, O. Corona, R. S. Correa, J. Ellena, M. R. Cominetti, A. A. Batista, M. Navarro, *Inorg. Chem.* **2017**, *56*, 3781–3793.
- [52] X. Zhao, R. Liu, Z. Chi, Y. Teng, P. Qin, *J. Phys. Chem. B* **2010**, *114*, 5625–5631.
- [53] J. Liu, J. N. Tian, J. Zhang, Z. Hu, X. Chen, *Anal. Bioanal. Chem.* **2003**, *376*, 864–867.
- [54] D. P. Tamboli, D. S. Lee, *J. Hazard. Mater.* **2013**, *260*, 878–884.
- [55] E. A. Masoud, A. M. Al-Hajry, A. Al-Marrani, *Int. J. Curr. Microbiol. Appl. Sci.* **2016**, *5*, 226.
- [56] A. K. Potbhare, M. S. Umekar, P. B. Chouke, M. B. Bagade, S. K. Tarik Aziz, A. A. Abdala, R. G. Chaudhary, *Mater. Today: Proc.* **2020**, *29*, 815–821.
- [57] P. B. Chouke, A. K. Potbhare, N. P. Meshram, M. M. Rai, K. M. Dadure, K. Chaudhary, A. R. Rai, M. F. Desimone, R. G. Chaudhary, D. T. Meshram, *ACS Omega* **2022**, *7*, 6869–6884.
- [58] W. Brand-Williams, M. E. Cuvelier, C. Berset, *Food Sci. Technol.* **1995**, *28*, 25–30.
- [59] P. Singla, V. Luxami, K. Paul, *Eur. J. Med. Chem.* **2016**, *117*, 59–69.
- [60] P. K. Sahu, P. K. Sahu, S. K. Gupta, D. Thavaselvam, D. D. Agarwal, *Eur. J. Med. Chem.* **2012**, *54*, 366–378.

Submitted: October 13, 2022

Accepted: December 2, 2022

RESEARCH ARTICLE



Curcumin caffeate (CCaf) polyphenol acts as an effective capping and reducing group in preparing stabilized AgNPs in aqueous medium and at room conditions. The process is eco-friendly owing to the no-toxicity of

CCaf and use of external chemical reductants. The AgNPs are found to have antioxidant, and antibacterial activity against ESKAPE bacterial pathogens and effective BSA binding interactions.

N. Gandha Gogoi, Prof. Dr. P. Dutta, Dr. J. Saikia, Prof. Dr. J. G. Handique**

1 – 9

Antioxidant, Antibacterial, and BSA Binding Properties of Curcumin Caffeate Capped Silver Nanoparticles Prepared by Greener Method



See discussions, stats, and author profiles for this publication at: <https://www.researchgate.net/publication/364312502>

MEDICINAL CHEMISTRY RESEARCH Enhanced biological activity of Curcumin Cinnamates: an experimental and computational analysis

Article in Medicinal Chemistry Research · October 2022

DOI: 10.1007/s00044-022-02977-w

CITATIONS

2

READS

155

6 authors, including:



Nishi Gandha Gogoi

MDKG College

6 PUBLICATIONS 8 CITATIONS

SEE PROFILE



Aziza Rahman

Dibrugarh University

11 PUBLICATIONS 26 CITATIONS

SEE PROFILE



Pankaj Dutta

Dibrugarh University

32 PUBLICATIONS 221 CITATIONS

SEE PROFILE



Anupaul Baruah

Dibrugarh University

21 PUBLICATIONS 136 CITATIONS

SEE PROFILE



Enhanced biological activity of Curcumin Cinnamates: an experimental and computational analysis

Nishi Gandha Gogoi¹ · Aziza Rahman¹ · Jiban Saikia¹ · Pankaj Dutta² · Anupaul Baruah¹ · Jyotirekha G. Handique¹

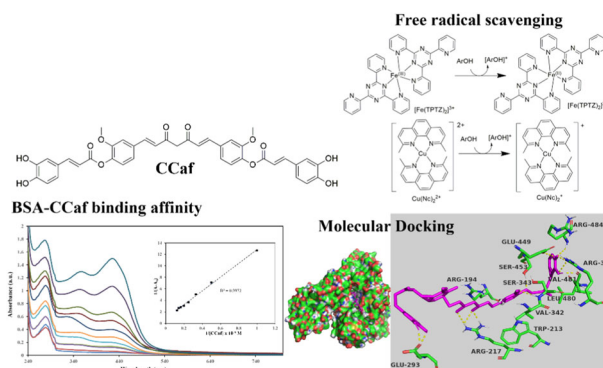
Received: 2 June 2022 / Accepted: 23 September 2022

© The Author(s), under exclusive licence to Springer Science+Business Media, LLC, part of Springer Nature 2022

Abstract

The binding of bioactive component in a drug molecule with proteins is important for their delivery at the target site in vivo. Bovine serum albumin (BSA) and human serum albumin (HSA) are mostly used as a preliminary benchmark model to study the protein-ligand binding affinity. In this work, we evaluated the biological activity of curcumin cinnamates (CCs) viz., curcumin ferulate (CFer), coumarate (CCou), caffeate (CCaf), and sinapate (CSin) derivatives. The binding interaction of these CCs as ligands with BSA and HSA is investigated by spectroscopic and in silico methods. The apparent binding constants of CCs are found to be in the range of $\sim 10^4$ – 10^5 M⁻¹ and are better compared to curcumin. The free radical scavenging property of CCs is evaluated by ferric reducing antioxidant power assay (FRAP) and cupric ion reducing antioxidant capacity (CUPRAC) methods. The antioxidant power of CCs is found to be higher than curcumin.

Graphical abstract



Keywords Curcumin · Curcumin cinnamates · Antioxidants · Serum albumins · Protein binding interaction · Molecular docking

Supplementary information The online version contains supplementary material available at <https://doi.org/10.1007/s00044-022-02977-w>.

✉ Anupaul Baruah
anupaulbaruah@dibru.ac.in

✉ Jyotirekha G. Handique
jghandique@rediffmail.com

Introduction

Polyphenolic antioxidants are gaining immense attention as nutraceuticals due to their wide medicinal applications in several neurodegenerative disorders, cancer, diabetes, and

¹ Department of Chemistry, Dibrugarh University, Dibrugarh 786004 Assam, India

² Department of Physics, Dibrugarh University, Dibrugarh 786004 Assam, India

cardiovascular diseases [1]. Polyphenols are grouped as one of the most important secondary plant metabolites [2] and play an effective role in maintaining the balance of the redox state of a cell by scavenging the free radicals, reactive oxygen and nitrogen species (ROS and RNS) [3]. The role of polyphenolic antioxidants as excellent hydrogen donors to the reactive radicals producing less reactive or non-reactive radicals [4] and protein binding mechanism are extensively explored in designing new drugs and preventive medicines [5, 6]. The number and positions of hydroxyl groups and the presence of other electron donating or withdrawing substituent determine the degree of enhancement in their reactivity [7]. Curcumin, a symmetrical conjugated β -diketonic polyphenolic antioxidant imparting a yellow-orange color to *Curcuma longa* has been traditionally explored in many medicinal applications from the ancient times [8]. Curcumin not only finds use as a culinary ingredient but also acts as anti-inflammatory, antimicrobial, anti-cancer, anti-viral, anti-HIV, anti-Alzheimer's and anti-depressant [9]. The phenolic hydroxyl groups are established to be responsible for its antioxidant behavior [10]. Many studies report the enhancement in aqueous solubility and biological profile of curcumin on esterification with other natural products and synthetic dendrimers [11–14]. Biodegradable curcumin conjugated diesters with glycine, valine, glutamic acid, and piperic acid show both antimicrobial and antiproliferative properties for their antioxidant and anti-inflammatory behavior and are much better compared to that of curcumin. Similarly, diglucoside of curcumin has better antimicrobial activity when compared to curcumin. The bioconjugates of curcumin act as pro-drugs as they get hydrolyzed and release the active drug at the target sites inside an infected cell. It can be attributed to the better solubility, cellular uptake and decreased metabolic degradation of these bioconjugates of curcumin in vivo [15–17].

Hydroxycinnamic acids (caffeic acid, ferulic acid, sinapic acid, and *p*-coumaric acid) (HCAs) are another class of natural phenolic compounds mostly found in plants and their products such as cereals, coffee, vegetables and fruits [18]. In nature, they mainly occur in esterified and conjugated forms [19]. Hydroxycinnamic acids and their derivatives are extensively studied due to their health beneficial effect as antioxidants in cancer, heart disease, neurological disorders, etc. mainly due to their hydrogen donating ability, supported by the stability of the resulting phenoxyl radical [20, 21].

Many polyphenols and their conjugates as antioxidants have been used as non-steroidal anti-inflammatory drugs (NSAIDs) for inflammation and pain. Inflammation is a normal and rapid biological response to a tissue damage, injury, chemical irritation, and infection by microbial pathogens [22]. This process is initiated by migration of the immune cells from both the adaptive and innate immune systems at the damaged site, followed by involvement of the

inflammatory cells and release of reactive oxygen and nitrogen radical species (ROS & RNS) and proinflammatory cytokines to neutralize the invading pathogens, repair injured tissues and assist wound healing [23]. The reactive radical species as H_2O_2 , $\bullet\text{O}_2^-$ (superoxide anion), OH (hydroxyl radical), NO and $^1\text{O}_2$ (singlet oxygen) are responsible for causing damage at the cellular and tissue sites by injuring the peptides, nucleic acids, and lipids in inflammatory cells. These in turn triggers signaling cascades, modulates inflammatory gene expression and production of inflammatory chemicals that causes oxidative damage at the normal tissues near the infected cells leading to extended inflammation [24, 25]. NSAIDs have significant importance in recovery of inflammation due to either injury or infection [26]. When delivered at the target site, NSAIDs works through inhibition of cyclooxygenase (COX) enzymes, primarily involved in biosynthesis of prostaglandins relieving swelling and pain. Binding ability of a bioactive part of a drug molecule with protein may have significant importance on the delivery, free concentration and metabolism of drug at the target site [27, 28]. Serum albumin in mammalian blood plasma has concentration of 50 mg mL^{-1} and is generally considered as a model system for studying the protein-drug interaction in vitro. Bovine serum albumin (BSA) has 583 amino acids with two tryptophan residues (Trp-134 and Trp-213) and phenylalanine at the binding pocket [29]. The human serum albumin (HSA) protein possesses 75% structural similarity to BSA [30]. The binding interactions of BSA/HSA and drug molecule can be investigated by UV-visible and fluorescence spectroscopic techniques by observing a change in the hyperchromicity in the absorption spectra of BSA-drug or HSA-drug complexes.

To the best of our knowledge, serum albumin interactions of curcumin cinnamates (CCs) are not attempted. In this work, we report the evaluation of antioxidant property of CCs in terms of equivalent concentration (EQ of $1 \text{ mM Fe}_2\text{SO}_4$) and trolox equivalent antioxidant capacity (TEAC). The binding affinities of curcumin and CCs to BSA and HSA are investigated by UV-visible and fluorescence spectroscopic techniques. The change in the microenvironment of active ligand binding site of BSA, and HSA in presence of CCs is investigated by in silico molecular docking.

Results and discussion

In a typical procedure, a reaction mixture of curcumin (1 mM) and HCAs (2 mM) is refluxed in ethanol at 60°C for 6 h in presence of a small amount of *p*-TsOH and under nitrogen atmosphere with constant stirring. The progress of reaction is monitored by examining TLC. A small amount of cold distilled water is added to the reaction medium and the ester so formed is separated by simple filtration method.

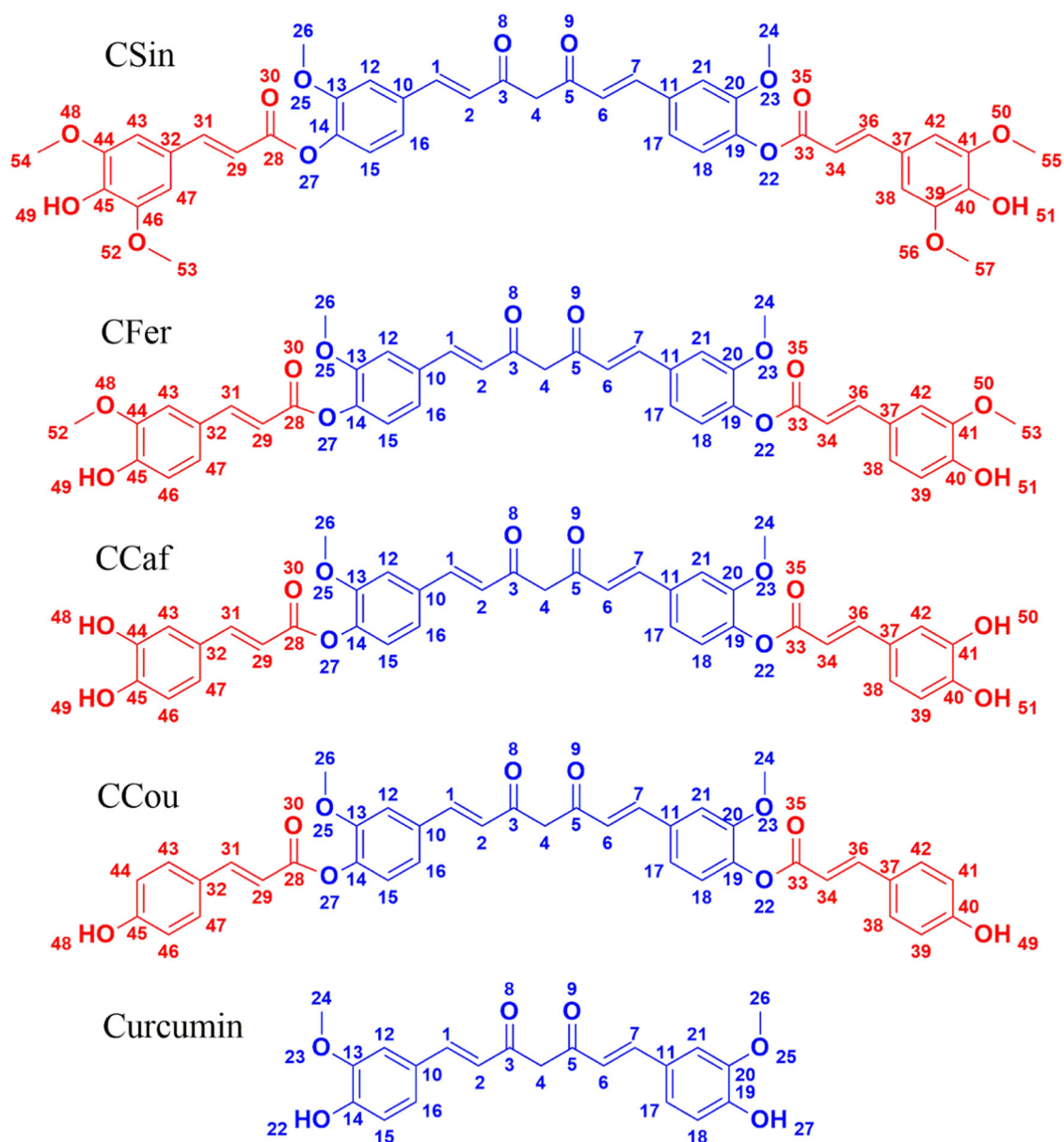


Fig. 1 Chemical structures of synthesized CCs and curcumin

The product is purified by column chromatography and characterized by UV-visible, FTIR, ^1H and ^{13}C NMR and LCMS analysis. Figure 1 shows the chemical structures of curcumin and synthesized CCs.

Antioxidant activity

The FRAP assay, based on electron transfer mechanism, is simple, easy and inexpensive method to evaluate the antioxidant activity of compounds. The results of FRAP assay are presented in Fig. 2 in terms of ferric equivalent concentration (EQ), defined as concentration of the antioxidant giving an equal amount of absorbance as given by 1 mM of

$\text{FeSO}_4 \cdot 7\text{H}_2\text{O}$. The higher the value of EQ (expressed in μM) lower is the antioxidant ability. The ease of electron donation by the antioxidants determines their reducing ability. The reducing ability of the antioxidants follows the order: $\text{CCaf} > \text{CSin} > \text{CFer} > \text{CCou} > \text{AscA} > \text{Curcumin}$. The EQ values of CCs are better compared to curcumin and ascorbic acid (standard). The number of phenolic hydroxyl groups, electron donating methoxy groups and conjugation in the structure of the antioxidants decides their enhancement in antioxidant activity [31]. The CCs retain their antioxidant behavior for a longer time and therefore might be able to show a protective effect against the oxidative damage of the food, if also used as food ingredients.

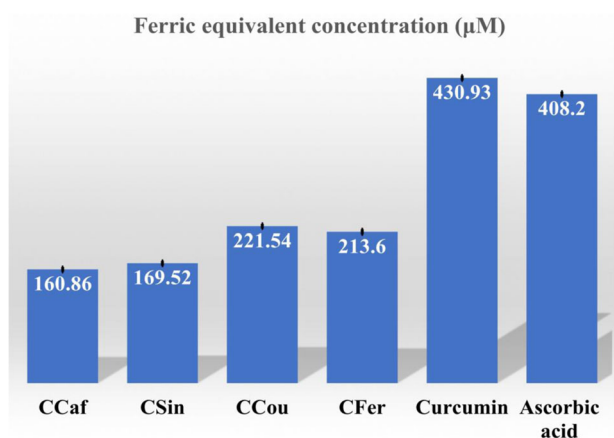


Fig. 2 Ferric equivalent concentrations (µM) of the antioxidants with the FRAP assay (mean ± SD, $n = 3$)

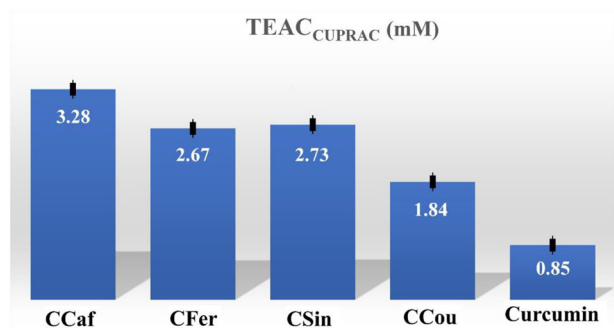


Fig. 3 TEAC coefficients (mM) of the antioxidants evaluated by CUPRAC assay (mean ± SD, $n = 3$)

The CUPRAC method introduced by Apak et al. 2008 [32], is a simple and versatile method studied for evaluating antioxidant capacity of many polyphenols, flavanoids, carotenoids, synthetic antioxidants, etc. The blue chromogen bis(neocuproine (Nc)) copper (II) cation $[\text{Cu}(\text{Nc})_2]^{2+}$ used in the CUPRAC assay oxidizes the reactive phenolic OH group (Ar-OH) of the antioxidants to the corresponding quinines (Ar=O), itself getting reduced to yellow-orange $\text{Cu}(\text{Nc})_2^+$ chelate. The antioxidant capacity of CCs evaluated by CUPRAC assay are expressed as TEAC coefficients i.e., the concentration of antioxidants giving the same reducing potency of the Cu^{2+} -Nc complex as 1 mM of trolox did at wavelength 450 nm. The antioxidant activities follow the trend: $\text{CCaf} > \text{CSin} > \text{CFer} > \text{CCou} > \text{Curcumin}$ (Fig. 3). The electron transfer mechanism involved in CUPRAC assay depends on the number and position of the phenolic hydroxy groups, electron donating methoxy groups and the conjugation allowing electronic delocalization in the structure of the antioxidants. The CCs are found to have higher activity compared to curcumin due to their extended conjugation in the whole structure.

Serum albumin protein binding study

UV-visible absorbance

The UV-visible absorption spectra measurements are carried out to examine the structural binding interaction of BSA and HSA with CCs and curcumin as ligands. BSA shows an absorption maximum at 280 nm and HSA at 277 nm in phosphate buffer solution (0.1 M, pH 7.4) due to $\pi \rightarrow \pi^*$ transition of the phenyl rings presents in chromophores-tyrosine (Tyr) tryptophan (Trp) and phenylalanine (Phe) residues [33–35]. The changes in the intensity band at 280 and 277 nm (hyperchromic or hypochromic and hypsochromic or bathochromic shift) is relevant to changes in the structure of BSA and HSA, particularly the hydrophobicity around Trp and Tyr residues [36]. In our work, the absorption intensity of BSA increases with increasing concentration of ligands and appearance of a new peak at 324 nm. This suggests concentration-dependent hyperchromic effect at 280 nm and formation of ground state complex due to binding interaction of BSA and ligands [37]. The maximum absorption wavelength of BSA at 280 nm undergoes hypsochromic shift with increasing concentrations of ligands indicating the change in micro-environment around Trp, Tyr and Phe groups in the binding pocket of BSA [38]. Figure 4 shows the absorption spectrum of BSA binding interaction with CCaf and the corresponding Benesi-Hildebrand plot of $1/(A_0 - A)$ versus $1/[\text{CCaf}]$. The apparent binding constant (K_{app}) calculated from Benesi-Hildebrand plot of BSA-ligand binding interaction are better for CCs than that of curcumin (See Table 1). The appearance of new band at 324 nm is not observed in case of curcumin. CCs and cur exhibit absorption peak around 433 and 420 nm respectively due to absorption of UV-light in this region.

Similarly, in case of HSA-ligand binding interaction the absorbance at 277 nm is found to increase with increase in concentration of ligand with simultaneous hypsochromic shift. The polarity around the microenvironment of Trp and Tyr residues are changed due to the interaction of HSA and ligands, with minor unfolding of the polypeptide backbone of HSA protein [35]. The absorbance spectrum of HSA and CCaf complexation and the corresponding Benesi-Hildebrand plot is shown in Fig. 4. The K_{app} values of CCs are higher than that of curcumin (see Table 1). The nature of complexation of BSA and HSA with CCs and curcumin is static as inferred from the change of absorption spectra of BSA in presence of ligand, which is altered in case of dynamic quenching as no such change in absorption spectra is observed in the vicinity of ligand [30, 39, 40].

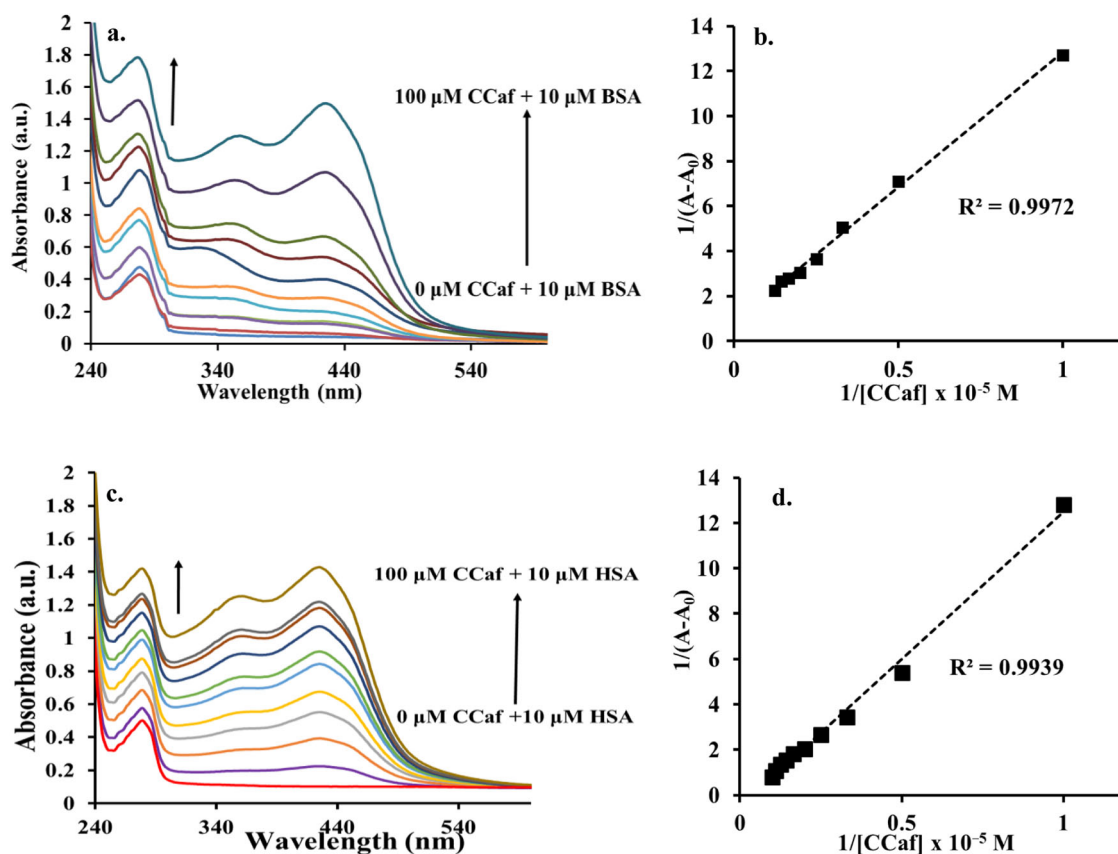


Fig. 4 **a** Absorbance spectra of BSA (10 μM) with CCaf (10–100 μM), and **(b)** Benesi-Hildebrand plot of $1/(A - A_0)$ vs. $1/[\text{CCaf}]$ for BSA; **(c)** absorbance spectra of HSA with CCaf (10–100 μM), and **(d)** Benesi-Hildebrand plot of $1/(A - A_0)$ vs. $1/[\text{CCaf}]$ for HSA

Table 1 Apparent binding constants of BSA-ligand and HSA-ligand interactions measured from UV-visible absorbance and fluorescence spectra

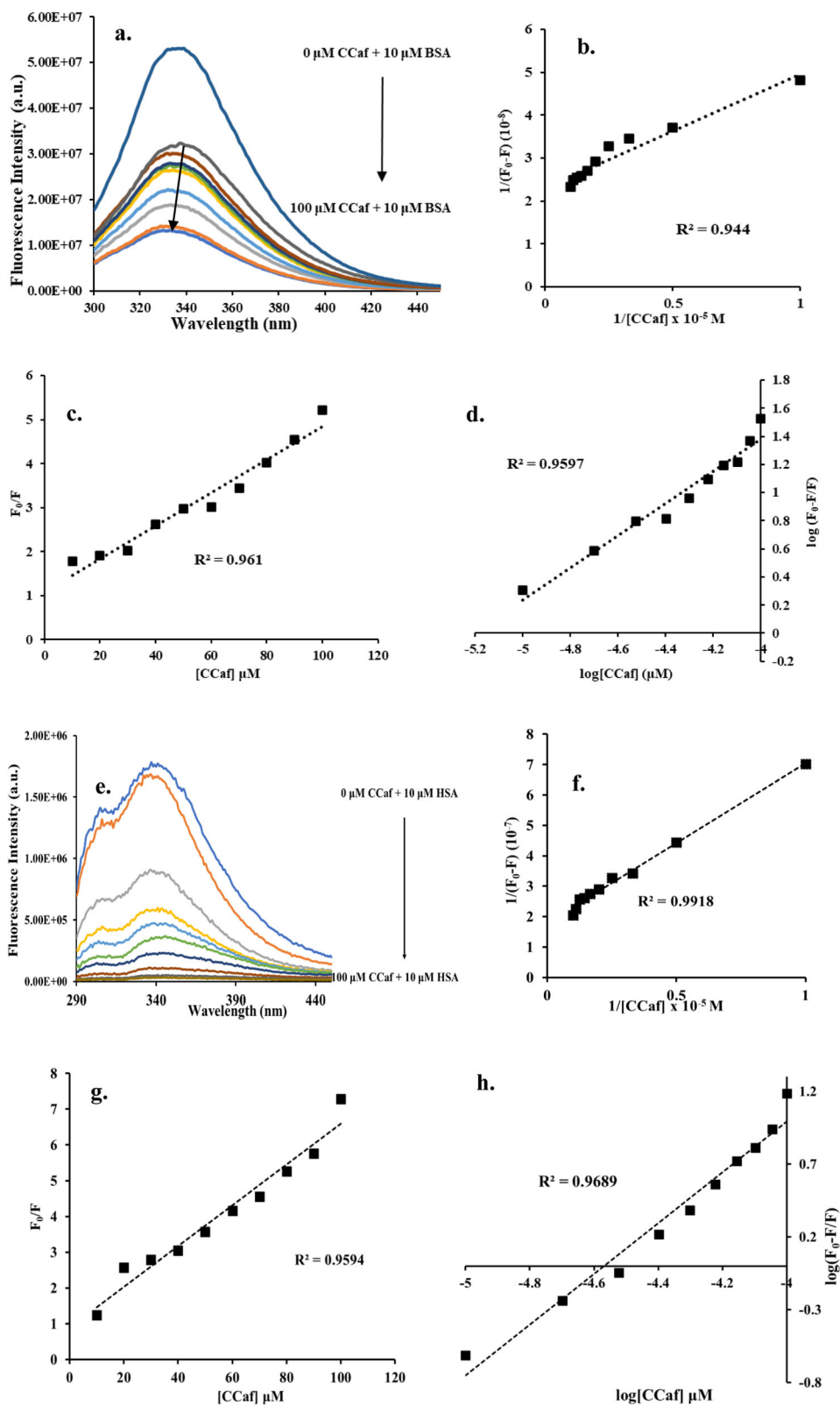
S. No.	BSA				HSA			
	K_{app} absorbance spectra (10^5 M^{-1})	K_{app} emission spectra (10^5 M^{-1})	No. of binding sites (n)	K_{SV} (10^5 M^{-1})	K_{app} (absorbance spectra, (10^5 M^{-1}))	K_{app} (emission spectra, (10^5 M^{-1}))	No. of binding sites (n)	K_{SV} (10^5 M^{-1})
CCaf	0.886	1.022	1.047	0.375	0.388	0.333	1.52	0.57
CCou	0.656	0.772	1.094	0.308	0.245	0.267	1.32	0.33
CSin	0.692	0.983	1.248	0.356	0.271	0.292	1.28	0.47
CFer	0.684	0.868	1.141	0.344	0.248	0.286	1.42	0.43
Curcumin	0.420	0.502	1.021	0.288	0.215	0.232	1.33	0.32

Steady state fluorescence emission

The fluorescence intensity of a fluorophore is quenched in presence of a ligand due to various molecular interactions such as energy transfer, molecular rearrangements, excited state reactions, formation of ground state complex (static quenching) or collisions among molecules (dynamic quenching) [41]. The fluorescence of BSA and HSA is observed due to the presence of three intrinsic fluorophores in their structure-Phe, Tyr and Trp. Out of the them, Trp is considered as the main contributor of fluorescence of BSA

and HSA as Phe and Tyr are opted out for low fluorescence quantum yield and high fluorescence quenching in presence of amino or carboxyl group, respectively [42]. Trp residue is highly sensitive to the minor change in hydrophobicity or polarity in its vicinity, and the fluorescence quenching is important in establishing the binding interaction of BSA and HSA in presence of ligands [43]. It is observed that with increase in concentration of ligands the fluorescence intensity of BSA and HSA decreases. Figure 5 shows the fluorescence emission spectra of CCaf and BSA and HSA binding interaction and the corresponding Benesi-

Fig. 5 **a** Emission spectra, **(b)** Benesi-Hildebrand plot of $1/(F_0 - F)$ vs. $1/[CCaf]$, **(c)** Stern-Volmer Plot, **(d)** double logarithmic plot of BSA ($10 \mu\text{M}$) with CCaf ($10\text{--}100 \mu\text{M}$); **(e)** emission spectra, **(f)** Benesi-Hildebrand plot of $1/(F_0 - F)$ vs. $1/[CCaf]$, **(g)** Stern-Volmer Plot, **(h)** double logarithmic plot of HSA ($10 \mu\text{M}$) with CCaf ($10\text{--}100 \mu\text{M}$)



Hildebrand plot of $1/(F_0 - F)$ versus $1/[CCaf]$ for BSA and HSA, where F_0 is the fluorescence intensity of BSA and HSA in absence of ligand and F is the fluorescence intensity

in presence of ligand. The K_{app} value of BSA-ligand binding from fluorescence spectra (Table 1) is found to be highest for CCaf ($1.022 \times 10^5 \text{ M}^{-1}$).

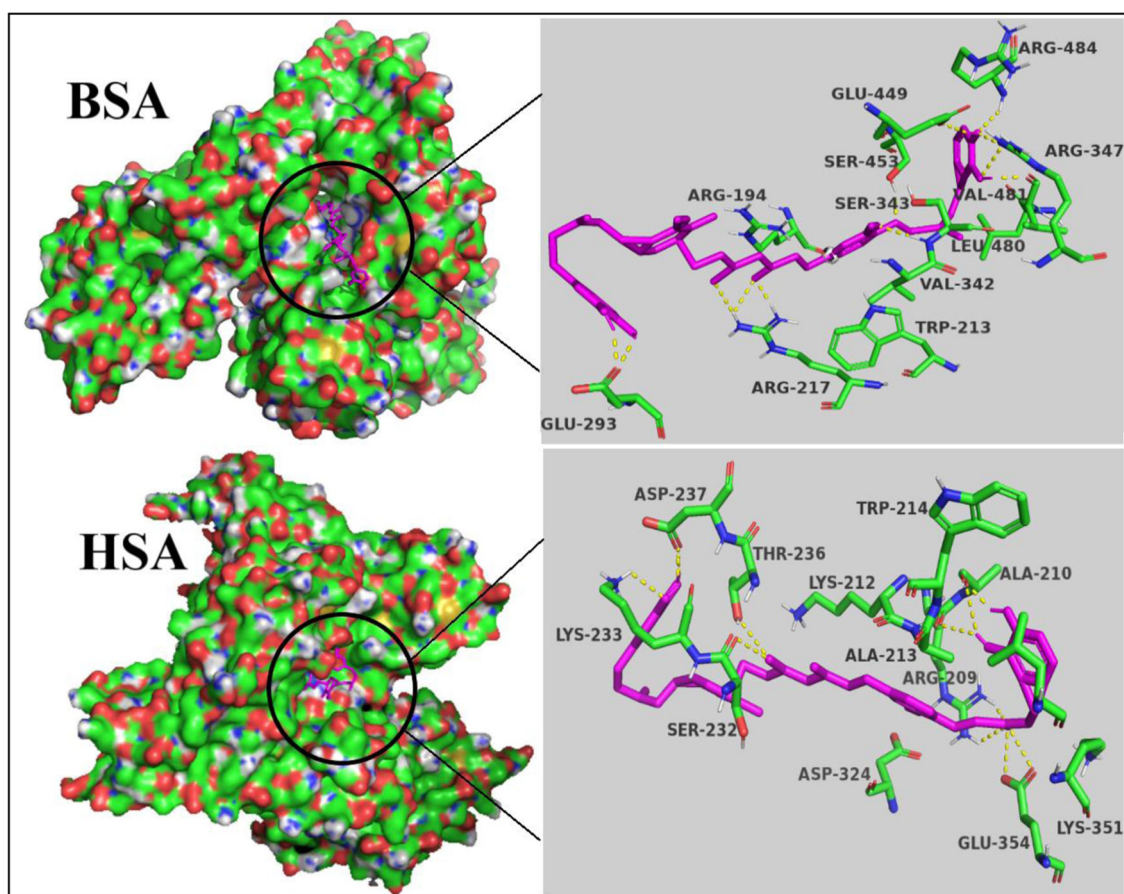


Fig. 6 The minimum energy docked conformations of CCaf with BSA, and HSA

The mechanism of protein-ligand quenching be either static quenching or dynamic quenching which is verified from the Stern-Volmer equation (Eq. 1.a).

$$F_0/F = K_{SV}[CCaf] + 1 \quad (1.a)$$

$$\text{Also,} \quad K_{SV} = K_q\tau_0 \quad (1.b)$$

where, F_0 and F are the fluorescence intensity of serum albumins in the absence and presence of CCaf ligand (quencher) and K_{SV} is the Stern-Volmer constant. K_q is the quenching constant and τ_0 is the average lifetime of the serum albumins (10^{-8} s for BSA and 2.02×10^{-10} s for HSA) [43, 44].

The plot of F_0/F vs. $[CCaf]$ for BSA gives a straight line, whose slope is equal to the value of K_{SV} ($0.375 \times 10^5 \text{ M}^{-1}$). The corresponding K_q value is $3.75 \times 10^{12} \text{ M}^{-1}\text{s}^{-1}$, which is greater than collision quenching constant $2.0 \times 10^{10} \text{ M}^{-1}\text{s}^{-1}$ [45]. In case of HSA, the K_{SV} value is $0.575 \times 10^5 \text{ M}^{-1}$ and the corresponding K_q value is measured to be $2.82 \times 10^{14} \text{ M}^{-1}\text{s}^{-1}$. Thus, the mechanism of quenching is confirmed to be static quenching due to formation of ground state complex between BSA/HSA and ligands and stabilized by non-covalent

interactions as hydrogen bonds, electrostatic, van der Waals or hydrophobic forces [46].

The modified Stern-Volmer equation gives the number of binding sites between the serum albumins and ligands (Eq. 2) [47].

$$\log(F_0 - F/F) = n \log[CCaf] + \log K_{app} \quad (2)$$

where n is the number of binding sites between CCaf and serum albumins obtained from the double logarithmic plot. CCs and curcumin are found to uniquely bind to both BSA and HSA (Table 1). The result of fluorescence spectroscopy is found to be in good agreement with the UV-visible absorbance spectroscopic result. The formation of ground state complex is concluded from the changes in the spectra of both the spectroscopic analysis. In support of the experimental findings on protein binding in silico docking study is also performed.

Docking studies

Molecular docking study is performed to understand the plausible interacting modes of the targeted molecules and serum albumins using co-crystal structures of BSA, and

HSA. Analysis of docking results is carried out using pymol. The docking score (in kcal/mol) and number of hydrogen bonds formed with the interacting amino acid residues at the binding site of the protein is determined. The docking result is shown in Figs. 6, S10–S13 (Supplementary Information) and Table 2. The spectroscopic and molecular docking results of curcumin and CCs as ligands with BSA protein complemented each other. There are two binding sites of BSA protein, namely the Sudlow's sites I and II, respectively located in the hydrophobic cavities of subdomain IIA and IIIA. The binding free energies (in kcal/mol) for protein-ligand complexes is obtained from the best energy ranked conformers. The polyphenols are reported to bind in the vicinity of Trp 213 of BSA [40]. CCs are found to bind at both sites of BSA, through hydrogen bonds and hydrophobic interactions with the surrounding amino acid residues of BSA. Among the synthesized esters, best binding energy is observed for CCaf -11.07 kcal/mol and least for CSin -10.13 kcal/mol. However, these values are better compared to that of curcumin -9.03 kcal/mol. BSA possess the polar amino acid residues on the surface while the hydrophobic amino acids with the aromatic groups are present inside the tertiary structure. The molecular docking results of HSA-ligand binding interactions are comparable to that of the BSA-ligand interactions. Curcumin and CCs are observed to be surrounded by the amino acid residues of the subdomain IIA and IIIA of HSA. The binding energy values of CCs are better compared to curcumin and the best binding energy value is observed for CCaf -11.06 kcal/mol. Thus, CCaf exhibits the best binding energy with both BSA and HSA amongst the CCs and curcumin, which is also in agreement with experimentally determined binding constants. The hydroxyl and keto groups on the ligand are involved in forming hydrogen bonds with the surrounding polar amino acids and the hydrophobic interactions takes place between the aromatic group of ligand and the hydrophobic amino acid residues on BSA and HSA. Earlier QSAR [48] and molecular docking studies [49–52] have also showed that number of aromatic rings, $-OH$ groups, H bonds, hydrophobic interactions etc are important attributes for BSA and HSA binding ligands. An analysis of the interactions shown in Table 2 imply that CCaf exhibits the best binding energy because of significantly more number of H bonds formed by CCaf due to the presence of two additional $-OH$ groups on the terminal benzene rings of CCaf compared to the other CCs and curcumin. This is clearly evident in the interactions shown in Table 2. The energetically best conformation of CCaf is forming 11 H bonds while the best conformations of the other three CCs have formed 5 to 7 H bonds and curcumin has formed 5 H bonds with BSA. In case of HSA CCaf exhibits 12 H bonds while the other three CCs exhibit 3 to 5 H bonds and curcumin forms 4 H bonds. It may be noted that in the

energetically best conformation of CCaf the keto groups (O8 and O9) are forming H-bond contact with Arg217 of BSA. However, the keto groups are present in all the ligands including curcumin and a closer analysis of the interactions in Table 2 shows that some of the other ligands are also forming H-bond contacts with BSA and HSA through either one or both the keto groups. Therefore we may conclude that involvement of the keto groups may not be the major reason behind CCaf being the best binding ligand. This again confirms that the two additional $-OH$ groups on CCaf and their additional H bonds which are absent in all the other four ligands is the reason for better binding of CCaf with BSA and HSA. Figure 6 shows the minimum energy docked conformation of CCaf with BSA and HSA. It is interesting to note that the number H bonds formed by curcumin and the CCs other than CCaf are comparable. However the CCs exhibits better binding energy compared to curcumin. We assign this better binding of CCs, to the fact that the CCs have more number of aromatic rings, larger size and occupy more space in the binding pockets of both BSA and HSA which may lead to more number of hydrophobic and other van der Waals interactions other than H bonds.

Another important point to note is that in Table 2 we provide the interactions made by the specific minimum energy conformation (in Supplementary Figs. S12, S13, this conformation is mentioned as conformation 1) for each ligand with BSA and HSA. However, in each of our docking simulations we generated 1000 conformations. AutoDock-GPU version: v1.5-release groups these 1000 conformations into different clusters meaning that structurally similar ligand conformations are grouped into a single cluster. It is commonly seen that even in a single cluster of conformations the specific interactions may vary conformation to conformation especially for large ligands with high torsional degrees of freedom. Earlier works [53, 54] also report that protein-ligand interactions can be dynamic rather than static due to structural flexibility of the ligands. Since the ligands developed in this work are relatively large with high torsional degrees of freedom, we observed that the conformations present in the same cluster as that of the best conformation shows slightly different binding interactions compared to the best conformation (see Supplementary Figs. S12, S13). This means that the interactions shown in Table 2, Figs. 6, S10–S13 are probable interactions which may be dynamically changing. This also implies that although from Table 2 data it may seem that structurally quite similar ligands like CCou and CCaf are exhibiting different interactions; if we consider the other conformations from the same cluster of the best conformations for these ligands the overall interactions may actually come out to be similar. The alternate conformations of CCou specifically exhibits some of the interactions exhibited by the

Table 2 Amino acid residues (within 3 Å of ligand), hydrogen bond interactions and the free energy of binding for the protein-ligand complexes of BSA and HSA from the best docking conformations

Ligand	BSA				HSA			
	Amino acids within 3 Å of ligand	Amino acids forming H bonds	$\Delta G_{\text{binding}}$ (kcal/mol)	Amino acids within 3 Å of ligand	Amino acids forming H bonds	$\Delta G_{\text{binding}}$ (kcal/mol)		
CCaf	Arg 194, Trp 213, Arg 217, Glu 293, Val 342, Ser 343, Arg 347, Glu 449, Ser 453, Leu 480, Val 481, Arg 484	O8...HN(Arg 217) O9...HN(Arg 217) OH48...O(Glu 293) OH49...O(Glu 293) OH50...HN(Arg 347) OH51...HN(Arg 347) OH51...O(Glu 449) O22...O(Ser 453) O23...HN(Leu 480) OH50...O(Val 481) OH51...HN(Arg 484) O30...O(Val 292) OH48...HN(Glu 293) OH49...HN(Arg 347) OH49...HN(Arg 483) OH49...HN(Arg 484) OH51...OH(Tyr 155) OH51...HN(Lys 159) O35...HN(Lys 187) O8...HN(Arg 217) OH49...HN(Arg 347) OH49...HN(Val 481) OH49...HN(Arg 484) O48...HO(Ser 201) O30...HN(Trp 213) O27...HN(Trp 213) OH49...O(Ala 209) OH51...HO(Glu 291) OH22...HN(Arg 198) O8...HO(Ser 343) O8...HO(Ser 453) OH27...HN(Arg 483) OH27...HN(Arg 484)	-11.07	Arg 209, Ala 213, Phe 211, Trp 214, Ser 232, Lys 233, Val 235, Thr 236, Asp 237, Leu 284, Asp 324, Leu 327, Leu 331, Glu 354	OH49...O(Arg 209) OH48...O(Ala 210) OH49...O(Ala 210) OH51...O(Ala 213) O9...O(Ser 232) OH50...N(Lys 233) O9...O(Thr 236) OH50...O(Asp 237) OH51...O(Asp 237) O30...NH(Asp 324) O30...O(Glu 354) O30...HO(Glu 354) OH49...HN(Arg 218) OH48...O(Gln 221) O9...O(Lys 444) OH49...O(Asp 451)	-11.06		
CCou	Arg 194, Leu 197, Trp 213, Arg 217, Glu 291, Val 292, Glu 293, Ser 343, Arg 347, Ser 453, Leu 480, Val 481, Arg 483, Arg 484	O30...O(Val 292) OH48...HN(Glu 293) OH49...HN(Arg 347) OH49...HN(Arg 483) OH49...HN(Arg 484) OH51...OH(Tyr 155) OH51...HN(Lys 159) O35...HN(Lys 187) O8...HN(Arg 217) OH49...HN(Arg 347) OH49...HN(Val 481) OH49...HN(Arg 484) O48...HO(Ser 201) O30...HN(Trp 213) O27...HN(Trp 213) OH49...O(Ala 209) OH51...HO(Glu 291) OH22...HN(Arg 198) O8...HO(Ser 343) O8...HO(Ser 453) OH27...HN(Arg 483) OH27...HN(Arg 484)	-10.82	Lys 195, Trp 214, Arg 218, Gln 221, Asn 295, Asp 296, Met 298, Asp 340, Val 343, Pro 447, Cys 448, Lys 444, Asp 451	-10.46			
CFer	Tyr 155, Lys 159, Lys 187, Trp 213, Arg 217, Val 342, Arg 347, Asp 450, Ser 453, Val 481, Arg 483, Arg 484	O35...HN(Lys 187) O8...HN(Arg 217) OH49...HN(Arg 347) OH49...HN(Val 481) OH49...HN(Arg 484) O48...HO(Ser 201) O30...HN(Trp 213) O27...HN(Trp 213) OH49...O(Ala 209) OH51...HO(Glu 291) OH22...HN(Arg 198) O8...HO(Ser 343) O8...HO(Ser 453) OH27...HN(Arg 483) OH27...HN(Arg 484)	-10.64	Glu 208, Arg 209, Lys 212, Trp 214, Val 216, Phe 228, Ala 229, Ser 232, Lys 233, Asp 237, Tyr 263, Asn 267	-9.37			
CSin	Ser 201, Ala 209, Leu 210, Trp 213, Arg 217, Glu 291, Lys 294, Val 342, Leu 346, Ser 453	O35...HN(Lys 187) O8...HN(Arg 217) OH49...HN(Arg 347) OH49...HN(Val 481) OH49...HN(Arg 484) O48...HO(Ser 201) O30...HN(Trp 213) O27...HN(Trp 213) OH49...O(Ala 209) OH51...HO(Glu 291) OH22...HN(Arg 198) O8...HO(Ser 343) O8...HO(Ser 453) OH27...HN(Arg 483) OH27...HN(Arg 484)	-10.13	Arg 209, Ala 225, Ser 232, Thr 236, Tyr 263, Glu 266, Asn 267	-9.80			
Curcumin	Arg 194, Arg 198, Trp 213, Leu 346, Arg 347, Ser 343, Ser 453, Leu 480, Val 481, Arg 483, Arg 484	O35...HN(Lys 187) O8...HN(Arg 217) OH49...HN(Arg 347) OH49...HN(Val 481) OH49...HN(Arg 484) O48...HO(Ser 201) O30...HN(Trp 213) O27...HN(Trp 213) OH49...O(Ala 209) OH51...HO(Glu 291) OH22...HN(Arg 198) O8...HO(Ser 343) O8...HO(Ser 453) OH27...HN(Arg 483) OH27...HN(Arg 484)	-9.03	Tyr 150, Lys 199, Arg 222, Leu 234, His 242, Arg 257, Leu 260, Ala 261, Ile 264, Ser 287	-8.66			

Atom numbers of the ligands given in the table are as mentioned in Fig. 1

best energy conformation of CCaf but not exhibited by the best energy conformation of CCou (see Supplementary Figs. S12, S13). Therefore, it may be again emphasized that the best binding energy of CCaf with both BSA and HSA is not due to some specific interaction but due to increase in the number of H bonds formed by the additional –OH groups.

Conclusions

In this work, four pharmacologically active derivatives of curcumin and hydroxycinnamic acids are reported with better antioxidant and anti-inflammatory properties compared to curcumin. The results of UV-visible absorbance spectra and fluorescence emission spectroscopy reveals that curcumin and CCs as ligand has the ability to bind with both BSA and HSA through formation of ground state complex between the serum albumins leading to static quenching. The binding constant of CCs are found to be higher than curcumin in both BSA and HSA. In silico molecular docking results indicate that curcumin and CCs could bind at the subdomain IIA and IIIA of BSA and HSA through formation of hydrogen bonds with the amino acid residues in those regions. The binding energy values calculated from the molecular docking studies are in close agreement with the experimental ones. This work can highlight the protein-ligand interaction of curcumin derivatives and provide important information in clinical research.

Experimental

Materials

Curcumin, ferulic acid, sinapic acid, caffeic acid, *p*-coumaric acid, trolox, BSA, and neocuproine (Nc) are purchased from Sigma Co. (MO, USA). 2,4,6-tri(2-pyridyl)-s-triazine (TPTZ) is obtained from TCI Chemicals (India) Pvt. Ltd and HSA from SRL, India. All other chemicals and solvents used are of analytical grade. The absorption spectra are recorded by a UV-Visible spectrophotometer (HITA-CHI U-3900H) over a wavelength range of 200–800 nm. For fluorescence emission spectroscopy, HORIBA Fluoromax-4 is used. ^1H NMR and ^{13}C NMR spectra are recorded on a Bruker Advance II 400 MHz model spectrometer in DMSO- d_6 as solvent using TMS as internal standard. Chemical shifts are reported downfield to TMS signal in parts per million (ppm). The resonant frequency of ^1H and ^{13}C is taken at 400 MHz and 100 MHz respectively. Molecular mass is recorded by Ultimate 3000/TSQ Endura liquid chromatograph mass spectrometer (LCMS).

Methods

Curcumin cinnamates are prepared by refluxing curcumin (1 mM) and hydroxycinnamic acid (2 mM) in ethanol at 60 °C for 6 h in presence of *p*-TsOH as catalyst. The solvent is removed under reduced pressure, product is washed with dilute acid and base solutions and filtered and dried. The purification of product is done by column chromatography.

(2E,2'E)-((1E,6E)-3,5-dioxohepta-1,6-diene-1,7-diyl)bis(2-methoxy-4,1-phenylene) bis(3-(4-hydroxy-3,5-dimethoxyphenyl)acrylate) (CSin)

Dark yellow solid. Yield: 0.556 g (71.3 %). ^1H NMR (400 MHz, DMSO- d_6) δ 7.65 (d, J = 16 Hz, =C–H) 7.54 (m, Ar–H), 7.24 (m, =C–H), 7.12 (d, J = 4 Hz, Ar–H), 6.95 (s, Ar–H), 6.86 (m, =C–H), 6.78 (m, Ar–H), 6.73 (d, J = 16 Hz, =C–H), 6.54 (s, Ar–H), 6.45 (dd, J = 4 Hz, Ar–H), 6.24 (d, J = 16 Hz, =C–H), 6.18 (s, Ar–H), 6.02 (s, Ar–H), 4.10 (m, –CH $_2$), 3.85 (m, –OCH $_3$); ^{13}C NMR (100 MHz, DMSO- d_6) δ 183.02 (–C=O), 167.19 (–O–C=O), 166.72 (–O–C=O), 149.70 (–C–OCH $_3$), 147.96 (–C–OCH $_3$), 145.36 (–C=), 140.64 (–C–OH), 138.26 (8, 8' –C=), 130.25 (–C=), 125.99 (Ar–C–O–C=O), 124.20 (–C=), 116.00 (Ar–C), 114.82 (Ar–C), 111.00 (Ar–C), 105.97, (Ar–C), 100.98 (Ar–C), 59.80 (–OCH $_3$), 55.95 (–OCH $_3$), 51.23 (–CH $_2$); LCMS (m/z): 779.46 [M–H] $^+$ (Calculated M^+ = 780.77).

(2E,2'E)-((1E,6E)-3,5-dioxohepta-1,6-diene-1,7-diyl)bis(2-methoxy-4,1-phenylene) bis(3-(4-hydroxy-3-methoxyphenyl)acrylate) (CFer)

Dark yellow solid. Yield: 0.506 g (70.2 %). ^1H NMR (400 MHz, DMSO- d_6) δ 7.54 (d, J = 16 Hz, =C–H), 7.25 (s, Ar–H), 7.12 (d, J = 8 Hz, Ar–H), 6.80 (d, J = 8 Hz, Ar–H), 6.70 (d, J = 16 Hz, =C–H), 6.63 (m, Ar–H), 6.57 (m, Ar–H) 6.40 (d, J = 16 Hz, =C–H), 6.24 (d, J = 16 Hz, =C–H), 6.04 (s, Ar–H), 5.83 (s, Ar–OH), 4.10 (s, –CH $_2$), 3.78 (m, –OCH $_3$); ^{13}C NMR (100 MHz, DMSO- d_6) δ 183.13 (–C=O), 167.21 (–O–C=O), 149.37 (–C–OCH $_3$), 147.49 (–C–OCH $_3$), 145.54 (–C–OH), 141.84 (Ar–C), 139.99 (Ar–C), 130.03 (–C=), 126.33 (–C=), 125.83 (Ar–C–O–C=O), 123.51 (–C=), 121.18 (Ar–C), 119.32 (Ar–C), 115.50 (Ar–C), 110.82 (Ar–C), 107.13 (Ar–C), 102.44 (Ar–C), 101.01 (Ar–C), 55.42 (–OCH $_3$), 51.25 (–CH $_2$); LCMS (m/z): 719.72 [M–H] $^+$ (Calculated M^+ = 720.22).

(2E,2'E)-((1E,6E)-3,5-dioxohepta-1,6-diene-1,7-diyl)bis(2-methoxy-4,1-phenylene) bis(3-(3,4-dihydroxyphenyl)acrylate) (CCaf)

Light orange solid. Yield: 0.484 g (70.1 %). ^1H NMR (400 MHz, DMSO- d_6) δ 7.50 (d, J = 12 Hz, =C–H), 7.26 (s,

Ar-H), 7.12 (dd, $J = 4$ Hz, 4 Hz, Ar-H), 6.80 (d, $J = 12$ Hz, Ar-H), 6.71 (d, $J = 16$ Hz, =C-H), 6.63 (m, Ar-H), 6.58 (m, Ar-H), 6.40 (d, $J = 16$ Hz, =C-H), 6.05 (s, Ar-H), 5.84 (s, Ar-OH), 4.11 (s, -CH₂), 3.79 (m, -OCH₃); ¹³C NMR (100 MHz, DMSO-d₆) δ 183.08 (-C=O), 168.56 (-O-C=O), 149.38 (-C-OCH₃), 147.52 (-C-OCH₃), 145.54 (-C-OH), 140.36 (Ar-C), 130.53 (Ar-C), 128.69 (Ar-C), 126.84 (C=), 125.35 (-C=), 123.02 (Ar-C-O-C=O), 121.16 (-C=), 116.00 (Ar-C), 111.32 (Ar-C), 108.50 (Ar-C), 102.85 (Ar-C), 101.48 (Ar-C), 55.43 (-OCH₃), 51.75 (-CH₂); LCMS (m/z): 691.44 [M-H]⁺ (Calculated M⁺ = 692.19).

(2E,2'E)-((1E,6E)-3,5-dioxohepta-1,6-diene-1,7-diyI)bis(2-methoxy-4,1-phenylene) bis(3-(4-hydroxyphenyl)acrylate) (CCou)

Dark yellow solid. Yield: 0.463 g (70.2 %). ¹H NMR (400 MHz, DMSO-d₆) δ 7.52 (d, $J = 12$ Hz, =C-H), 7.25 (s, Ar-H), 7.11 (d, $J = 8$ Hz, Ar-H), 6.80 (d, $J = 8$ Hz, Ar-H), 6.76 (m, Ar-H), 6.71 (d, $J = 16$ Hz, =C-H), 6.64 (m, Ar-H), 6.55 (m, Ar-H), 6.32 (d, $J = 16$ Hz, =C-H), 6.26 (d, $J = 16$ Hz, =C-H), 6.08 (s, Ar-H), 5.82 (s, Ar-OH), 4.12 (s, -CH₂), 3.82 (s, -OCH₃); ¹³C NMR (100 MHz, DMSO-d₆) δ 183.54 (-C=O), 168.08 (-O-C=O), 149.85 (-C-OCH₃), 147.90 (-C-OCH₃), 145.04 (-C-OH), 140.88 (Ar-C), 130.06 (Ar-C), 126.83 (-C=), 123.52 (-C=), 121.18 (Ar-C-O-C=O), 114.63 (-C=), 113.65 (Ar-C), 111.32 (Ar-C), 108.48 (Ar-C), 103.31 (Ar-C), 101.46 (Ar-C), 55.43 (-OCH₃), 51.77 (-CH₂); LCMS (m/z): 659.77 [M-H]⁺ (Calculated M⁺ = 660.67).

The stock solution of CCs and trolox (as standard) are prepared at a concentration of 10 mM in DMSO and diluted further to 10–100 μ M concentrations with DMSO solution for antioxidant study and with phosphate buffer saline solution (0.1 M PBS; pH = 7.4) for serum albumin binding study. BSA/HSA standard solution is prepared at a concentration of 10 μ M in PBS solution.

FRAP assay

The antioxidant capacity of each concentration of test sample solutions is estimated by FRAP assay according to the original method described [55] with some modifications. The working solution of FRAP reagent under acidic conditions (pH 3.6) is prepared by mixing 2.5 mL of 10 mmol/L TPTZ solution in 40 mmol/L HCl, 2.5 mL of 20 mmol/L FeCl₃·6H₂O and 25 mL of 300 mmol/L acetate buffer solution (3.1 g CH₃COONa·3H₂O and 16 mL CH₃COOH per litre of buffer solution). An amount of freshly prepared reagent (2.4 mL) is incubated at 37 °C and absorbance at 593 nm is recorded as reagent blank. 0.6 mL of test sample solution of

concentration range 10–100 μ M is added to 2.4 mL of the reagent. The change in absorbance (ΔA) of the reaction mixture is proportional to the reducing/antioxidant power of the antioxidants and is measured as an increase in absorbance at λ 593 nm due to reduction of [Fe(III)(TPTZ)₂]³⁺ to the blue colored [Fe(II)(TPTZ)₂]²⁺ ferrous complex (Fig. 7).

CUPRAC assay

The procedure of CUPRAC assay is followed from the method reported in literature [56]. 1.0×10^{-2} M of CuCl₂ solution is prepared by dissolving 0.4262 g CuCl₂·2H₂O in water and diluting to 250 mL. Ammonium acetate (NH₄OAc) buffer (pH 7.0) at concentration of 1.0 M is prepared by dissolving 19.27 g NH₄OAc in water and diluting to 250 mL. Neocuproine (Nc) solution, 7.5×10^{-3} M, is prepared by dissolving 0.039 g Nc in 96% ethanol, and diluting to 25 mL with ethanol. The CUPRAC method can be applied as four interrelated procedures, i.e., normal (N), incubated (I), hydrolyzed (H), and hydrolyzed and incubated (H&I) versions of the assay. In our present work, we applied the normal sample measurement procedure of the CUPRAC assay. The standard calibration curves of each antioxidant compound are generated by plotting absorbance versus molar concentration, and the molar absorptivity of the CUPRAC method for each antioxidant is found from the slope of the calibration line concerned. The scheme for the normal measurement of hydrophilic antioxidants is summarized as: 1 mL Cu(II) + 1 mL Nc + 1 mL buffer + x mL antioxidant solution + (1.0 - x) mL H₂O; total volume = 4.0 mL. The reaction mixture is incubated at 37 °C for 30 min and heated at 50 °C in water bath until the solution develop a light blue color, and then measured absorbance at 450 nm. The reaction is based on reduction of light blue colored [Cu(Nc)₂]²⁺ to yellow colored [Cu(Nc)₂]⁺ complex (Fig. 7). Trolox Equivalent Antioxidant Capacity (TEAC) values (Eq. 3) of phenolic antioxidants in CUPRAC method is calculated as the ratio of molar absorptivity of the antioxidant versus the molar absorptivity of trolox:

$$TEAC_{A.O} = \epsilon A.O / \epsilon Trolox \quad (3)$$

where, $\epsilon A.O$ is the molar absorptivity of the phenolic antioxidant and $\epsilon Trolox$ is the molar absorptivity of trolox.

Serum albumin binding study

The binding interactions of BSA and HSA with CCs and curcumin as ligands is studied by observing the change in absorption and emission spectra of BSA and HSA in presence of different concentrations of ligands. The working solution is prepared by addition of 2 mL of BSA/HSA [prepared in phosphate buffer solution (PBS); pH 7.4], 0.5 mL of ligand and 0.5 mL of PBS. The concentration of BSA/HSA is fixed

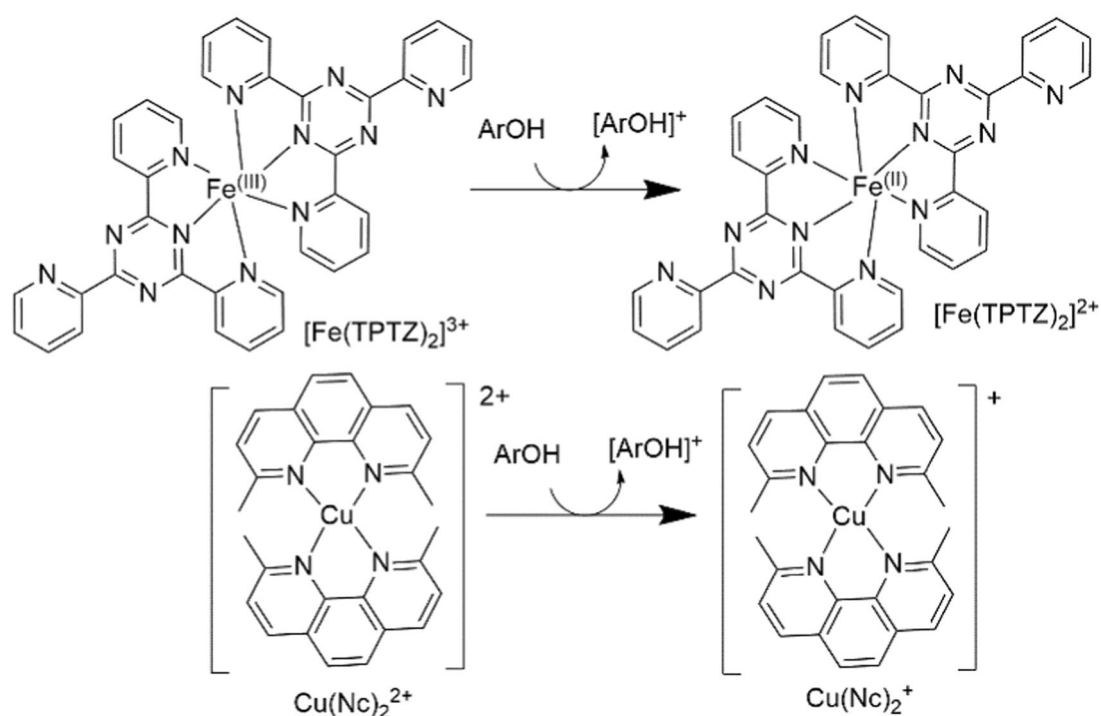


Fig. 7 FRAP and CUPRAC reaction mechanism with antioxidants (ArOH)

at $10 \mu\text{M}$. The solution is incubated for 30 mins at 37°C . The binding constant (K_{app}) is calculated from absorption data by Benesi-Hindeland equation (Eq. 4).

$$\frac{1}{(A_{\text{obs}} - A_0)} = \frac{1}{(A_C - A_0)} + \frac{1}{K_{\text{app}}(A_C - A_0)[\text{ligand}]} \quad (4)$$

where, A_{obs} is the absorbance observed for BSA/HSA with different concentrations of ligand; A_0 is the blank absorbance of BSA/HSA; A_C is the maximum absorbance of BSA/HSA with ligand; K_{app} is the apparent binding constant. A graph is plotted between $1/(A_{\text{obs}} - A_0)$ versus $1/[\text{CCs}]$ and $1/(F_0 - F)$ versus $1/[\text{CCs}]$ and the ratio of intercept to slope of the linear fit plot gave the K_{app} of BSA/HSA and ligand.

Molecular docking

All docking calculations were performed on a Linux 64 operating system using AutoDock-GPU version: v1.5-release [57] in order to gain insights into the binding modes and binding affinity of curcumin and CCs with BSA and HSA. The preparation of proteins and ligands are done using AutoDock Tools version 1.5.7 [58]. The X-ray crystal structures for these proteins are retrieved from the protein data bank (PDB) with PDB ID: 4F5S(A) and 4K2C(A) respectively. The structure of curcumin and CCs as ligand are generated in Avogadro followed by energy minimization. All other ligands, and water molecules are removed followed by addition of

polar hydrogen atoms to the protein structure. Considering the ligand molecules as flexible and the protein as rigid, both proteins are docked to each of the five ligands using autodock force field. 1000 conformations are generated from each docking simulation. The top 5 conformers are analysed and the best among them is selected for further study. The visualization of the docked conformations and the evaluation of the protein-ligand interactions are performed in PyMOL [59].

Acknowledgements Authors are grateful to the UGC, New-Delhi for Special Assistance Program (SAP-DRS) and Department of Science and Technology (DST), Govt. of India, for financial assistance under DST-FIST program to the Department of Chemistry, Dibrugarh University. NGG acknowledges DUREF, Dibrugarh University for financial assistance. AR and AB acknowledge UGC, India (Project No: 30-406/2017 (BSR)) and DST-SERB (Project No. ECR/2017/000494) for financial support.

Compliance with ethical standards

Conflict of interest The authors declare no competing interests.

References

- Santhakumar AB, Battino M, Alvarez-Suarez JM. Dietary polyphenols: structures, bioavailability and protective effects against atherosclerosis. *Food Chem Toxicol.* 2018;113:49–65.
- Luca SV, Macovei I, Bujor A, Miron A, Skalicka-Wozniak K, Aprotosoaie AC, et al. Bioactivity of dietary polyphenols: the role of metabolites. *Crit Rev Food Sci Nutr.* 2020;60:626–59.

- Hunyadi A. The mechanism(s) of action of antioxidants: From scavenging reactive oxygen/nitrogen species to redox signalling and the generation of bioactive secondary metabolites. *Med Res Rev.* 2019;39:2505–33.
- Serrelli G, Deiana M. In vivo formed metabolites of polyphenols and their biological efficacy. *Food Funct.* 2019;10:6999–7021.
- Lacroix S, Badoux JK, Scott-Boyer MP, Parolo S, Matone A, Priami C, et al. A computationally driven analysis of the polyphenol-protein interactome. *Sci Rep.* 2018;8:2232.
- Chen J, Yang J, Ma L, Li J, Shahzad N, Kim CK. Structure-antioxidant activity relationship of methoxy, phenolic hydroxyl, and carboxylic acid groups of phenolic acids. *Sci Rep.* 2020;10:2611.
- Sun YM, Zhang HY, Chen DZ, Liu CB. Theoretical elucidation on the antioxidant mechanism of curcumin: a DFT study. *Org Lett.* 2002;4:2909–11.
- Nelson KM, Dahlin JL, Bisson J, Graham J, Pauli GF, Walters MA. The essential medicinal chemistry of Curcumin. *J Med Chem.* 2017;60:1620–37.
- Gera M, Sharma N, Ghosh M, Huynh DL, Lee SJ, Min T, et al. Nanoformulation of curcumin: an emerging paradigm for improved remedial application. *Oncotarget.* 2017;8:66680–98.
- Sarkar N, Bose S. Liposome-encapsulated curcumin-loaded 3D printed scaffold for bone tissue engineering. *ACS Appl Mater Interfaces.* 2019;11:17184–92.
- Khayyal MT, El-Hazek RM, El-Sabbagh WA, Frank J, Behnam D, Abdel-Tawab M. Micellar solubilisation enhances the anti-inflammatory activities of curcumin and boswellic acids in rats with adjuvant-induced arthritis. *Nutrition* 2018;54:189–96.
- Alven S, Nqoro X, Aderibigbe BA. Polymer-based materials loaded with curcumin for wound healing applications. *Polymers* 2020;12:2286.
- Misra S, Narain U, Misra R, Misra K. Design, development and synthesis of mixed bioconjugates of piperic acid-glycine, curcumin-glycine/alanine and curcumin-glycine piperic acid and their antibacterial and antifungal properties. *Bioorg Med Chem.* 2005;13:1477.
- Pavathy KS, Negi PS, Srinivas P. Antioxidant, antimutagenic, and antibacterial activities of curcumin- β -diglucoside. *Food Chem.* 2009;111:265.
- Dubey SK, Sharma AK, Narain U, Misra K, Pati U. Design, synthesis and characterization of some bioactive conjugates of curcumin glycine, glutamic acid, valine, and demethylated piperic acid and study their antimicrobial and antiproliferative properties. *Eur J Med Chem.* 2008;43:1837.
- Rashmi HB, Negi PS. Phenolic acids from vegetables: a review on processing stability and health benefits. *Food Res Int.* 2020;136:109298.
- Maurya DK, Devasagayam TPA. Antioxidant and prooxidant nature of hydroxycinnamic acid derivatives ferulic and caffeic acids. *Food Chem Toxicol.* 2010;48:3369–73.
- Conman V, Vodnar DC. Hydroxycinnamic acids and human health: recent advances. *J Sci Food Agric.* 2020;100:483–99.
- Sova M, Saso L. Natural sources, pharmacokinetics, biological activities and health benefits of hydroxycinnamic acids and their metabolites. *Nutrients* 2020;12:2190.
- Pan MH, Lai CS, Ho CT. Anti-inflammatory activity of natural dietary flavonoids. *Food Funct.* 2010;1:15–31.
- Chu C, Artis D, Chiu IM. Neuro-immune interactions in the tissues. *Immunity* 2020;52:464–74.
- Chuang YC, Chang HM, Li CY, Cui Y, Lee CL, Chen CS. Reactive oxygen species and inflammatory responses of macrophages to substrates with physiological stiffness. *ACS Appl Mater Interfaces.* 2020;12:48432–41.
- Maleki SJ, Crespo JF, Cabanilas B. Anti-inflammatory effects of flavonoids. *Food Chem.* 2019;299:125124.
- Hameister R, Kaur C, Dheen ST, Lohmann CH, Singh G. Reactive oxygen/nitrogen species (ROS/RNS) and oxidative stress in arthroplasty. *J Biomed Mater Res B.* 2020;108:2073–87.
- Raghuvanshi DS, Verma N, Singh S, Luqman S, Gupta AC, Bawankule DU, et al. Design and synthesis of novel oleanolic acid based chromenes as anti-proliferative and anti-inflammatory agents. *N J Chem.* 2018;42:16782–94.
- Wang J, Sun H, Li Y, Chu H, Sun J. Synthesis and preliminary anti-inflammatory activity exploration of novel derivatives of kirenel. *N J Chem.* 2020;44:19250–61.
- Bindu S, Mazumder S, Bandopadhyay U. Non-steroidal anti-inflammatory drugs (NSAIDs) and organ damage: a current perspective. *Biochem Pharmacol.* 2020;180:114147.
- Ambati GG, Jachack SM. Natural product inhibitors of cyclooxygenase (COX) enzyme: A review on current status and future perspectives. *Curr Med Chem.* 2021;28:1877–905.
- Rouzer CA, Marnett LJ. Structural and chemical biology of the cyclooxygenase with substrates and non-steroidal anti-inflammatory drugs. *Chem Rev.* 2020;120:7592–641.
- Singla P, Luxami V, Paul K. Synthesis and in vitro evaluation of novel triazine analogues as anticancer agents and their interaction studies with bovine serum albumin. *Eur J Med Chem.* 2016;117:59–69.
- Parolia S, Maley J, Sammynaiken R, Green R, Nickerson M, Ghosh S. Structure-functionality of lentil protein-polyphenol conjugates. *Food Chem.* 2022;367:130603.
- Apak R, Güçlü K, Özyürek M, Çelik SE. Mechanism of antioxidant capacity assays and the CUPRAC (cupric ion reducing antioxidant capacity) assay. *Microchim Acta.* 2008;160:413.
- Qureshi MA, Javed S. Aflatoxin B1 induced structural and conformational changes in bovine serum albumin: A multi-spectroscopic and circular dichroism-based study. *ACS Omega.* 2021;6:18054–64.
- Pawar SK, Jaldappagari S. Interaction of repaglinide with bovine serum albumin: spectroscopic and molecular docking approaches. *J Pharm Anal.* 2019;9:274–83.
- Anand K, Rajamanikandan R, Selva Sharma A, Ilanchelian M, Khan FI, Tiloke C, et al. Human serum albumin interaction, in silico and anticancer evaluation of pine-gold nanoparticles. *Process Biochem.* 2020;89:98–109.
- Siddiqui S, Ameen F, Kausar T, Nayeem SM, Ur Rehman S, Tabish M. Biophysical insight into the binding mechanism of doxofylline to bovine serum albumin: An in vitro and in silico approach. *Spectrochim Acta Part A* 2021;249:119296.
- Phopin K, Ruankham W, Prachayasittikul S, Prachayasittikul V, Tantimongkolwat T. Insight into the molecular interaction of cloxyquin (5-Chloro-8-Hydroxyquinoline) with bovine serum albumin: biophysical analysis and computational simulation. *Int J Mol Sci.* 2020;21:249.
- Satish L, Millan S, Bera K, Mohapatra S, Sahoo H. A spectroscopic and molecular dynamic simulation approach towards the stabilizing effect of ammonium based ionic liquids on bovine serum albumin. *N J Chem.* 2017;41:10712–22.
- Gadallah MI, Ali HRH, Askal HF, Saleh GA. Towards understanding the interaction of certain carbapenems with protein via combined experimental and theoretical approach. *Spectrochim Acta Part A.* 2021;246:119005.
- Skrť M, Benedik E, Podlipnik C, Ulrih NP. Interactions of different polyphenols with bovine serum albumin using fluorescence quenching and molecular docking. *Food Chem.* 2012;135:2418–24.
- Paul BK, Bhattacharjee K, Bose S, Guchhait NA. Spectroscopic investigation on the interaction of a magnetic ferrofluid with a model plasma protein: Effect on the conformation and activity of the protein. *Phys Chem Chem Phys.* 2012;14:15482–93.

42. Sułkowska A. Interaction of drugs with bovine and human serum albumin. *J Mol Struct.* 2002;614:227–32.
43. Mittal A, Gandhi S, Roy I. Mechanistic interaction studies of synthesized ZIF-8 nanoparticles with bovine serum albumin using spectroscopic and molecular docking approaches. *Sci Rep.* 2022;12:10331.
44. Villarreal W, Colina-Vegas L, Visbal G, Corona O, Correa RS, Ellena J, et al. Copper(I)–Phosphine polypyridyl complexes: Synthesis, characterization, DNA/HSA binding study, and anti-proliferative activity. *Inorg Chem.* 2017;56:3781–93.
45. Zhao X, Liu, Chi Z, Teng Y, Qin P. New insights into the behavior of bovine serum albumin adsorbed onto carbon nanotubes: comprehensive spectroscopic studies. *J Phys Chem B.* 2010;114:5625–31.
46. Ware WR. Oxygen quenching of fluorescence in solution: an experimental study of the diffusion process. *J Phys Chem.* 1962;66:455–8.
47. Liu J, Tian JN, Zhang J, Hu Z, Chen X. Interaction of magnolol with bovine serum albumin: A fluorescence-quenching study. *Anal Bioanal Chem.* 2003;376:864–7.
48. Votano JR, Parham M, Hall LM, Hall LH, Kier LB, Oloff S, et al. QSAR modeling of human serum protein binding with several modeling techniques utilizing structure-information representation. *J Med Chem.* 2006;49:7169–81.
49. Roy S, Nandi RK, Ganai S, Majumdar KC, Das TK. Binding interaction of phosphorus heterocycles with bovine serum albumin: a biochemical study. *J Pharm Anal.* 2017;7:19–26.
50. Jin XL, Wei X, Qi FM, Yu SS, Zhou B, Bai S. Characterization of hydroxycinnamic acid derivatives binding to bovine serum albumin. *Org Biomol Chem.* 2012;10:3424–31.
51. Khan MW, Al Otaibi A, Al-Zahrani SA, Alshammari EM, Haque A, Alouffi S, et al. Experimental and theoretical insight into resistance to glycation of bovine serum albumin. *J Mol Struct.* 2021;1230:129645.
52. Wani TA, Bakheit AH, Zargar S, Bhat MA, Al-Majed AA. Molecular docking and experimental investigation of new indole derivative cyclooxygenase inhibitor to probe its binding mechanism with bovine serum albumin. *Bioorg Chem.* 2019;89:103010.
53. Kandasamy S, Chinnasamy K, Poomani K. Understanding the conformational flexibility and electrostatic properties of curcumin in the active site of rhAChE via molecular docking, molecular dynamics and charge density analysis. *J Biomol Struct Dyn.* 2017;35:3627–47.
54. Hughes TS, Chalmers MJ, Novick S, Kuruvilla DS, Chang MR, Kamenecka TM, et al. Ligand and receptor dynamics contribute to the mechanism of graded PPAR γ agonism. *Structure.* 2012;20:139–50.
55. Benzie IFF, Strain JJ. Ferric reducing/antioxidant power assay: direct measure of total antioxidant activity of biological fluids and modified version for simultaneous measurement of total antioxidant power and ascorbic acid concentration. *Methods Enzym.* 1999;15:299.
56. Özyürek M, Güçlü K, Tütem E, Başkan KS, Erçağ E, Celik SE, et al. A comprehensive review of CUPRAC methodology. *Anal Methods.* 2011;11:2439.
57. Santos-Martins D, Solis-Vasquez L, Tillack AF, Sanner MF, Koch A, Forli S. Accelerating AutoDock4 with GPUs and gradient-based local search. *J Chem Theory Comput.* 2021;17:1060–73.
58. Morris GM, Huey R, Lindstrom W, Sanner MF, Belew RK, Goodsell DS, et al. AutoDock4 and AutoDockTools4: Automated docking with selective receptor flexibility. *J Comput Chem.* 2009;30:2785–91.
59. DeLano WL. Pymol: an open-source molecular graphics tool. *CCP4 Newsl Protein Crystallogr.* 2002;40:82–92.

Publisher's note Springer Nature remains neutral with regard to jurisdictional claims in published maps and institutional affiliations.

Springer Nature or its licensor holds exclusive rights to this article under a publishing agreement with the author(s) or other rightsholder(s); author self-archiving of the accepted manuscript version of this article is solely governed by the terms of such publishing agreement and applicable law.